

An interpretable neural network-based non-proportional odds model for ordinal regression with continuous response

Akifumi Okuno^{1,2} and Kazuharu Harada^{3,1}

¹The Institute of Statistical Mathematics

²RIKEN Center for Advanced Intelligence Project

³Tokyo Medical University

okuno@ism.ac.jp, haradak@tokyo-med.ac.jp

Abstract

This study proposes an interpretable neural network-based non-proportional odds model (N³POM) for ordinal regression. In the model, the response variable can take continuous values, and the regression coefficients vary depending on the predicting ordinal response. Contrary to conventional approaches, where the linear coefficients of regression are directly estimated from the discrete response, we train a non-linear neural network that outputs the linear coefficients by taking the response as its input. By virtue of the neural network, N³POM may have flexibility while preserving the interpretability of the conventional ordinal regression. We show a sufficient condition under which the predicted conditional cumulative probability (CCP) locally satisfies the monotonicity constraint over a user-specified region in the covariate space. We also provide a monotonicity-preserving stochastic (MPS) algorithm for adequately training the neural network.

Keywords: Continuous ordinal regression, Non-proportional odds model, Neural network

1 Introduction

Ordinal regression modeling treats response as an ordinal scale and aims to understand the relationship between the response order and covariates (Agresti, 2010). In the context of ordinal regression modeling, response variables are typically assumed to be ordinal and discrete (e.g., stage of cancer, scores of wine quality). While standard regression-based approaches are mainly interested in the actual value of the response, this study focuses on thresholds of the responses; that is, the probability of the response being less than or equal to a specific threshold as a function of the covariates.

Let $d, J \in \mathbb{N}$ and consider (G, X) , a pair of such discrete ordinal response variables $G \in \{1, 2, \dots, J\}$ and their covariate $X \in \mathbb{R}^d$. A standard model for analyzing such a threshold is the proportional odds model (POM):

$$\text{logit}(\mathbb{P}_{\text{POM}}(G \leq j \mid X = \mathbf{x})) = \alpha_j + \langle \boldsymbol{\beta}, \mathbf{x} \rangle \quad (j \in \{1, 2, \dots, J-1\}),$$

where $\text{logit}(z) = \log \frac{z}{1-z}$ is a logit function, and $\alpha_1, \alpha_2, \dots, \alpha_{J-1} \in \mathbb{R}$, $\boldsymbol{\beta} \in \mathbb{R}^d$ are parameters to be estimated. This model satisfies the parallelism assumption (McCullagh, 1980), which states that the regression coefficients are equal across all thresholds. However, the parallelism assumption is often considered to be violated (see, e.g., Long and Freese (2006)). For example, in restaurant ratings, basic factors such as good hygiene may be considered important in lower scores, while factors like ingredient origin and wine selection may be considered more significant in higher scores. See Williams (2016) for a discussion on the violation of the parallelism assumption in a real-world situation.

One approach to circumvent the assumption violation is leveraging the non-proportional odds model (NPOM, a.k.a., generalized ordinal logit model):

$$\text{logit}(\mathbb{P}_{\text{NPOM}}(G \leq j \mid X = \mathbf{x})) = \alpha_j + \langle \boldsymbol{\beta}_j, \mathbf{x} \rangle \quad (j \in \{1, 2, \dots, J-1\}),$$

that allows the coefficients to vary across the response thresholds. See, for example, [McCullagh and Nelder \(1989\)](#), [Peterson and Harrell \(1990\)](#), and [Williams \(2006\)](#). However, there remain several difficulties in leveraging NPOM.

- (D-1) The first difficulty is the lack of monotonicity of the predicted conditional cumulative probability (CCP); that is, the predicted CCP may violate monotonicity as $\hat{\mathbb{P}}_{\text{NPOM}}(G \leq j \mid X = \mathbf{x}) > \hat{\mathbb{P}}_{\text{NPOM}}(G \leq j+1 \mid X = \mathbf{x})$ for some (j, \mathbf{x}) , because of the flexibility of the varying coefficients ([Tutz and Berger, 2022](#); [Lu et al., 2022](#)). Given that simple POM with $\alpha_1 \leq \alpha_2 \leq \dots \leq \alpha_{J-1}$ is monotone in terms of the CCP, [Lu et al. \(2022\)](#) considers $\boldsymbol{\beta}_j = \boldsymbol{\beta}_* + \boldsymbol{\delta}_j$ with a prototype $\boldsymbol{\beta}_*$ and incorporates L^2 penalty in the deviation $\boldsymbol{\delta}_j$. [Wurm et al. \(2021\)](#) (a.k.a. ordinalNet) incorporates elastic penalty, which is the sum of L^2 and L^1 penalties. [Tutz and Berger \(2022\)](#) further restricts the deviation as $\boldsymbol{\delta}_j = (j - J/2)\boldsymbol{\delta}$. They have asserted that a monotone CCP is obtained by increasing the penalty weights as the NPOM then gets closer to the simple POM, estimating only the prototype. However, the larger penalty weights may yield a larger bias, while smaller weights do not guarantee monotonicity; thus, specifying the proper penalty weights remains a problem.
- (D-2) The second difficulty is the lack of the proximity guarantee of the estimated coefficients for adjacent thresholds. Given that it is more natural for the adjacent coefficients to be proximate, [Tutz and Gertheiss \(2016\)](#) and [Ugba et al. \(2021\)](#) incorporate a penalty between the coefficients of adjacent thresholds $\|\boldsymbol{\beta}_{j+1} - \boldsymbol{\beta}_j\|_2^2$. However, the adjacent penalty cannot be simply incorporated into the aforementioned monotonicity-guaranteed NPOM because of its incompatibility with the optimization algorithm.
- (D-3) The third difficulty is the lack of extensibility to continuous responses. In some cases, we are interested in the probability that a continuous variable (e.g., item prices, lifetime of people) is less than or equal to a threshold. Existing methods used to train the NPOM, which directly estimate countably many coefficients $\boldsymbol{\beta}_1, \boldsymbol{\beta}_2, \dots, \boldsymbol{\beta}_J$, cannot be simply extended to the continuous response; a naive extension needs to estimate uncountably many coefficients $\{\boldsymbol{\beta}_u\}_{1 \leq u \leq J}$. As a study in the field of survival analysis, [Satoh et al. \(2016\)](#) relaxes the parallelism assumption in the continuous POM ([Bennett, 1983](#); [Kalbfleisch and Prentice, 2002](#)). However, no monotonicity guarantee is provided therein. See Section 2.3 for details.

Our study is the first to simultaneously address all of these three difficulties. Accordingly, we propose a *neural network-based NPOM* (N^3POM):

$$\text{logit}(\mathbb{P}_{\text{N}^3\text{POM}}(H \leq u \mid X = \mathbf{x})) = a(u) + \langle \mathbf{b}(u), \mathbf{x} \rangle \quad (u \in [1, J]),$$

where $H \in [1, J]$ is a continuous response variable associated with the covariate $X \in \mathbb{R}^d$ and $a : [1, J] \rightarrow \mathbb{R}$ is a piece-wise linear continuous function. We employ a non-linear neural network for the coefficient $\mathbf{b} : [1, J] \rightarrow \mathbb{R}^d$. Thus, continuity is naturally introduced to the varying coefficients. Given that we train the neural network for estimating the coefficients of the linear model instead of directly modeling the cumulative probability, the proposed N^3POM preserves the interpretability of the conventional POM and NPOM. We also provide a sufficient condition of the functions a, \mathbf{b} to satisfy the monotonicity constraint of the predicted CCP. Using this constraint, we propose a *monotonicity-preserving stochastic* (MPS) algorithm, which trains the parametric functions a, \mathbf{b} by maximizing the weighted log-likelihood through the stochastic gradient ascent algorithm. Figure 1 illustrates the comparison of POM, NPOM, and N^3POM (proposal). N^3POM demonstrates better scores than existing POM and NPOM in synthetic dataset experiments. We apply N^3POM to several real-world datasets.

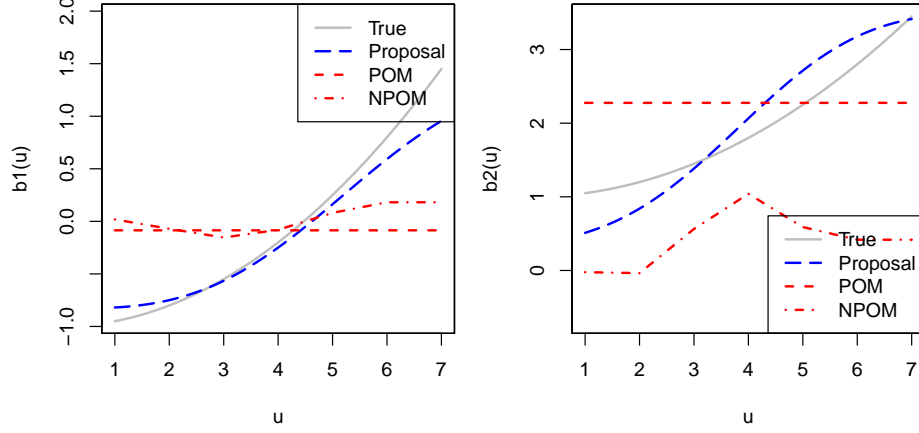


Figure 1: Illustration of N³POM. Grey lines represent the true coefficients $\mathbf{b}_*(u) = (b_{*1}(u), b_{*2}(u)) = (-1 + 0.05u^2, 1 + 0.05u^2)$, blue lines represent the estimated coefficients $\hat{\mathbf{b}}(u)$ of the proposed N³POM, red lines represent the coefficients of existing POM implemented by `polr` function in R language and NPOM implemented by `ordinalNet` function equipped with ridge penalty (with only the non-parallel terms). The coefficients of POM and NPOM are linearly interpolated. This illustration corresponds to an instance in the synthetic dataset experiments. See Section 4 for details.

2 Preliminaries and Related Works

Section 2.1–2.3 summarize problem-setting, symbols, and related works, respectively.

2.1 Problem setting

This section describes the problem-setting of this study. Let $n, d, J \in \mathbb{N}$ and $H \in \mathcal{U} := [1, J]$ be a random variable representing an ordered response associated with a covariate $X \in \mathbb{R}^d$. Let $\{(h_i, \mathbf{x}_i)\}_{i=1}^n \subset \mathcal{U} \times \mathbb{R}^d$ be n i.i.d. observations of the pair (H, X) . Next, using the observations, this study aims to interpret the relationship between the covariate X and the response H , through the prediction of the logit function applied to the conditional cumulative probability (CCP)

$$\text{logit}(\mathbb{P}(H \leq u \mid X = \mathbf{x})), \quad (u \in \mathcal{U} = [1, J]) \quad (1)$$

(or equivalently, $\text{logit}(\mathbb{P}(H > u \mid X = \mathbf{x}))$). Particularly, the estimated CCP $\hat{\mathbb{P}}(H \leq u \mid X = \mathbf{x})$ is expected to be non-decreasing with respect to $u \in \mathcal{U}$, for fixed \mathbf{x} . Throughout this study, the non-decreasing property is also simply referred to as monotonicity.

2.2 Symbols

This study uses the following symbols. $\sigma(z) = 1/(1 + \exp(-z))$ represents a sigmoid function, $\text{logit}(z) = \sigma^{-1}(z) = \log \frac{z}{1-z}$ represents a logit function, $\rho : \mathbb{R} \rightarrow \mathbb{R}$ denotes a user-specified activation function of the neural network (i.e., $\rho(z) = \tanh(z)$), and $\rho^{[1]}(z) = \rho'(z)$, $\rho^{[2]}(z) = \rho''(z)$ denote the first- and second-order derivatives. $\|\mathbf{x}\|_p = \{x_1^p + x_2^p + \dots + x_d^p\}^{1/p}$ for $\mathbf{x} = (x_1, x_2, \dots, x_d)$, $p \in \mathbb{N}$. $\langle \mathbf{x}, \mathbf{x}' \rangle = \mathbf{x}^\top \mathbf{x}'$ denotes an inner product of the vectors \mathbf{x}, \mathbf{x}' . \emptyset , which denotes an empty set.

For clarity, $\nabla_{\boldsymbol{\theta}}$, ∇_u are called by different names as the gradient (with respect to $\boldsymbol{\theta}$) and derivative (with respect to u), respectively. Particularly, for any function $f : \mathcal{U} \rightarrow \mathbb{R}$, $f^{[1]} : \mathcal{U} \rightarrow \mathbb{R}$ is called a weak derivative of f , if $f(u) = f(1) + \int_1^u f^{[1]}(\tilde{u}) d\tilde{u}$ holds for any $u \in \mathcal{U}$. If f is differentiable almost everywhere over \mathcal{U} , $f^{[1]}$ is compatible with $\nabla_u f(u)$ except for all the (non-measurable) indifferentiable points in f ; $f^{[1]}$ can be defined even if f is indifferentiable at some points. Note that the weak derivative of f is generally not unique, which is why we define a weak derivative for each function.

2.3 Related works

Among the several types of ordinal regression models, such as the continuation-ratio logit and adjacent-categories logit models (Agresti, 2010), this study focuses on the cumulative logit model. We herein describe the related works on non-linear extensions of ordinal regression, continuous extensions of ordinal regression (more specifically, continuous extensions of NPOM), and monotone neural network.

Non-linear extensions of ordinal regression

Ordinal regression has been extended to non-linear models; for example, Chu and Ghahramani (2005) for Gaussian process, and Cardoso and da Costa (2007) for neural networks. In line with the POM, the linear model $f_j^{(\text{lin.})}(\mathbf{x}) = \alpha_j + \langle \boldsymbol{\beta}, \mathbf{x} \rangle$ has been extended to non-linear models $f_j^{(\text{n-lin.})}(\mathbf{x}) = \alpha_j + m(\mathbf{x})$; Vargas et al. (2019) and Vargas et al. (2020) employ a neural network for m , and simple intercept model in Kook et al. (2022b) employs a partially non-linear function $f_j^{(\text{pn-lin.})}(\mathbf{x}) = \alpha_j + \langle \boldsymbol{\beta}, \mathbf{x}' \rangle + \tilde{m}(\mathbf{x}'')$ for $\mathbf{x} = (\mathbf{x}', \mathbf{x}'')$, where \mathbf{x}' denote observed covariate elements whose relation to the response is of interest, and \mathbf{x}'' is the remaining observed covariate elements. See Herzog et al. (2022) for its medical application. Kook et al. (2022b) also indicates that neural additive model $f_j^{(\text{add.})}(\mathbf{x}) = \alpha_j + \sum_{k=1}^d \tilde{m}_k(x_k)$ (Agarwal et al., 2021) equipped with neural networks \tilde{m}_k can be employed for POM. However, the aforementioned approaches consider (non-linear) prediction models f that are independent of the threshold j ; they cannot capture the local relationship between the covariates and the response for each threshold j .

Kook et al. (2022b) also proposes a complex intercept (CI) model $f_j^{(\text{CI})}(\mathbf{x}) = \alpha_0(\mathbf{x}) + \sum_{c=1}^j \exp(\gamma_c(\mathbf{x}))$ with non-linear functions $\{\gamma_c\}_{c=1}^J$. This model can be regarded as a response-dependent prediction model (i.e., a non-linear extension of NPOM). While this CI model is guaranteed to be monotone for increasing $j = 1, 2, \dots, J$ and they have high expressive power, the model cannot be extended to continuous response (as we cannot estimate uncountable many functions $\{\gamma_c\}_{c \in [1, J]}$), and it is hard to interpret the relationship between the covariates and the response, through the estimated non-linear functions γ_c .

Continuous extensions of ordinal regression

In line with ordinal regression, not many studies have examined continuous response. Thas et al. (2012) proposes a probabilistic index model, which models the pairwise ordinal relationship $\mathbb{P}(H_i \leq H_j \mid X_i = \mathbf{x}_i, X_j = \mathbf{x}_j)$, and Liu et al. (2017) extends POM to a continuous response with a non-specific cumulative link function, even though both of these studies assume parallel regression coefficients.

In other areas, survival analysis has much in common with ordinal regression with continuous response. A widely-used model in survival analysis is the Cox's model, which leverages the covariate X . Cox's model is a semi-parametric function

$$\lambda_{\text{Cox}}(u \mid X = \mathbf{x}) = \lambda_0(u) \exp(\langle \boldsymbol{\gamma}_{\text{Cox}}(u), \mathbf{x} \rangle)$$

that approximates the following hazard function:

$$\lambda(u \mid X = \mathbf{x}) := \frac{q(u \mid X = \mathbf{x})}{\mathbb{P}(H > u \mid X = \mathbf{x})} = -\frac{\frac{d}{du} \{1 - \mathbb{P}(H \leq u \mid X = \mathbf{x})\}}{1 - \mathbb{P}(H \leq u \mid X = \mathbf{x})} = -\frac{d}{du} \log \{1 - \mathbb{P}(H \leq u \mid X = \mathbf{x})\}, \quad (2)$$

where $u \geq 0$ is regarded as a time-point in survival analysis, and $\lambda_0(u)$ is a non-negative baseline-hazard function. While the standard Cox's model employs a constant coefficient (i.e., there exists a vector $\boldsymbol{\gamma}$ such that $\boldsymbol{\gamma}_{\text{Cox}}(u) = \boldsymbol{\gamma}$ for all u), we consider a response-dependent (non-constant) coefficient $\boldsymbol{\gamma}_{\text{Cox}}(u)$ for comparison. For such a flexible coefficient function, see, for example, Hastie and Tibshirani (1993). Solving the differential equation (2) yields the CCP

$$\mathbb{P}_{\text{Cox}}(H \leq u \mid X = \mathbf{x}) = 1 - \exp\left(-\int_0^u \lambda_{\text{Cox}}(\tilde{u} \mid X = \mathbf{x}) d\tilde{u}\right) = 1 - \exp\left(-\int_0^u \lambda_0(\tilde{u}) \exp(\langle \boldsymbol{\gamma}_{\text{Cox}}(\tilde{u}), \mathbf{x} \rangle) d\tilde{u}\right). \quad (3)$$

However, compared to our model (7) defined later in Section 3.1, it is hard to interpret the coefficient $\gamma_{\text{Cox}}(u)$ from the perspective of the CCP (3). Furthermore, most survival analysis methods focus more on hazard function estimation instead of estimating CCP.

Continuous extensions of NPOM

Regarding the CCP estimation leveraging the covariates, in the context of the survival analysis, [Bennett \(1983\)](#) defines a log-logistic regression model: $\text{logit}(\mathbb{P}_{\text{Bennett}}(H \leq u \mid X = \mathbf{x})) = a \log u + \langle \mathbf{b}, \mathbf{x} \rangle$. While this model and its variants assume parallel regression coefficients \mathbf{b} (see, e.g., [Kalbfleisch and Prentice \(2002\)](#) for a comprehensive survey), [Satoh et al. \(2016\)](#) further modifies this simple model to

$$\text{logit}(\mathbb{P}_{\text{Satoh}}(H \leq u \mid X = \mathbf{x})) = a_{\text{Satoh}}(u) + \langle \mathbf{b}_{\text{Satoh}}(u), \mathbf{x} \rangle, \quad (u \in [1, J]), \quad (4)$$

which is also called the time-varying coefficient model. Therein, the functions $a_{\text{Satoh}}, \mathbf{b}_{\text{Satoh}}$ are defined by polynomial functions $a_{\text{Satoh}}(u) = \sum_{\ell=1}^L u^{\ell-1} \tilde{a}_{\ell}, \mathbf{b}_{\text{Satoh}}(u) := \sum_{\ell=1}^L u^{\ell-1} \tilde{\mathbf{b}}_{\ell}$, where $\{\tilde{a}_{\ell}\}_{\ell=1}^L \subset \mathbb{R}, \{\tilde{\mathbf{b}}_{\ell}\}_{\ell=1}^L \subset \mathbb{R}^d$ are parameters to be estimated. However, unfortunately, any sufficient condition to guarantee the monotonicity of the model (4) is not provided in [Satoh et al. \(2016\)](#). However, our model (7) is proved to be monotone when the covariate belongs to $\chi_2(\eta) := \{\mathbf{x} \in \mathbb{R}^d \mid \|\mathbf{x}\|_2 \leq \eta\}$, as discussed in Section 3.2. As a counterexample of monotonicity, (4) reduces to a function $\sigma(a_{\text{Satoh}}(u) + \langle \mathbf{b}_{\text{Satoh}}(u), \mathbf{x} \rangle) = \sigma((u-2)(u-3))$ not monotone with respect to $u > 0$ for all $\mathbf{x} \in \mathbb{R}^d$ (i.e., invalid as an estimator of CCP), by specifying $a_{\text{Satoh}}(u) = (u-2)(u-3)$ (i.e., $\tilde{a}_1 = 6, \tilde{a}_2 = -5, \tilde{a}_3 = 1, \tilde{a}_4 = \tilde{a}_5 = \dots = 0$) and $\mathbf{b}_{\text{Satoh}}(u) = \mathbf{0}$ (i.e., $\tilde{\mathbf{b}}_1 = \dots = \tilde{\mathbf{b}}_L = \mathbf{0}$).

As a promising work partially sharing the common purposes with ours, deep conditional transformation models (DCTM; [Baumann et al., 2021](#)), that is implemented as the `deeptrafo` package in R language ([Kook et al., 2022a](#)), is equivalent to a probabilistic model

$$\text{logit}(\mathbb{P}_{\text{DCTM}}(H \leq u \mid X = \mathbf{x})) = \langle \mathbf{b}_{\text{DCTM}}(u), \mathbf{c}_{\text{DCTM}}(\mathbf{x}) \rangle + e_{\text{DCTM}}(\mathbf{x}), \quad (u \in [1, J]) \quad (5)$$

where $\mathbf{c}_{\text{DCTM}}(\mathbf{x})$ is a parametric transformation function to be estimated (they employ deep NN for this function $\mathbf{c}_{\text{DCTM}}(\mathbf{x})$). Also $\mathbf{b}_{\text{DCTM}}, e_{\text{DCTM}}$ are parametric functions defined by

$$\mathbf{b}_{\text{DCTM}}(u) := \Theta^\top \tilde{\mathbf{b}} \left(\frac{u-1}{J-1} \right), \quad e_{\text{DCTM}}(\mathbf{x}) := \langle \boldsymbol{\phi}, \tilde{\mathbf{e}}(\mathbf{x}) \rangle.$$

$\tilde{\mathbf{b}}(\tilde{u}) = (\tilde{b}_1(\tilde{u}), \dots, \tilde{b}_L(\tilde{u}))$ and $\tilde{\mathbf{e}}(\mathbf{x}) = (\tilde{e}_1(\mathbf{x}), \dots, \tilde{e}_L(\mathbf{x}))$ are concatenations of preliminarily specified basis functions, and $\Theta = (\theta_{ij}), \boldsymbol{\phi} = (\phi_i)$ are parameters to be estimated. [Baumann et al. \(2021\)](#) and [Kook et al. \(2022b\)](#) employ the Bernstein basis functions ([Farouki, 2012](#)); more specifically, probability density function of the Beta distribution $\text{Beta}(\ell, L-\ell)$ is employed for the function $\tilde{b}_{\ell}(u)$. As also discussed in [Sick et al. \(2021\)](#), DCTM (5) equipped with the Bernstein basis functions is guaranteed to be monotone (for $u \in [1, J]$ with fixed \mathbf{x}) if $\mathbf{s}(\mathbf{x}) = (s_1(\mathbf{x}), s_2(\mathbf{x}), \dots, s_L(\mathbf{x})) := \Theta \mathbf{c}_{\text{DCTM}}(\mathbf{x})$ is monotonically increasing, i.e.,

$$s_1(\mathbf{x}) \leq s_2(\mathbf{x}) \leq \dots \leq s_L(\mathbf{x}). \quad (6)$$

Therefore, studies in line with [Sick et al. \(2021\)](#), [Baumann et al. \(2021\)](#), and [Kook et al. \(2022b\)](#) estimate the parameter Θ of the Bernstein basis functions so as to satisfy the monotonicity (6). However, existence of the parameter Θ satisfying the monotonicity (6) (for all \mathbf{x}) depends on the choice of $\mathbf{c}_{\text{DCTM}}(\mathbf{x}) = (c_1(\mathbf{x}), \dots, c_L(\mathbf{x}))$; such Θ does not exist if we employ the simple identity transformation $\mathbf{c}_{\text{DCTM}}(\mathbf{x}) = \mathbf{x}$ considered in this paper, as $\mathbf{s}(-\mathbf{x}) = -\mathbf{s}(\mathbf{x})$ is monotonically decreasing (i.e., (6) is not satisfied) if $\mathbf{s}(\mathbf{x})$ satisfies (6). Although a positive mapping such as $c_i(\mathbf{x}) = \exp(\gamma_i(\mathbf{x}))$ using a deep neural network γ_i (considered in [Baumann et al. \(2021\)](#)) can address this issue, this approach is not compatible with our problem setting, as it estimates the function c_i while we fix the function $c_i(\mathbf{x}) = x_i$ for interpretability.

Monotone neural network

Regarding the monotonicity-introduced models, we last discuss the relation to the partially monotone neural network (Daniels and Velikova, 2010), that is another (potentially) possible model for estimating the CCP. Daniels and Velikova (2010) extends the univariate min-max network (Sill, 1997) to multivariate settings, and proves its monotonicity and universal approximation capability. While the totally monotone neural network considers the monotonicity over (u, \mathbf{x}) , monotonicity for \mathbf{x} is not required in our problem setting; the partially monotone neural network is more flexible and is guaranteed to be monotone with respect to only the partial input u . You et al. (2017) provides a more flexible partially monotone deep neural network called deep lattice network. Liu et al. (2020) also provides a mixed integer linear programming framework, that trains general neural networks using piece-wise linear activation functions (e.g., deep NN using ReLU activation function) to be partially monotone. However, the aforementioned approaches also lack the interpretability of the relation between the observed covariate \mathbf{x} and the response u .

3 Proposed Model

This section proposes a novel ordinal regression model for continuous response. We describe the proposed N³POM in Section 3.1 and the monotonicity of N³POM in Section 3.2. Based on the aforementioned model endowed with monotonicity, we provide a parameter estimation algorithm in Section 3.3. Finally, we discuss the adaptation to the discrete responses in Section 3.4.

3.1 Neural network-based non-proportional odds model (N³POM)

To simultaneously address the difficulties (D-1), lack of monotonicity in the predicted CCP, (D-2) lack of proximity guarantee in the estimated coefficients for adjacent thresholds, and (D-3) lack of extensibility to continuous responses, which are explained in the Introduction, we propose a *neural network-based non-proportional odds model* (N³POM):

$$\text{logit}(\mathbb{P}_{\text{N}^3\text{POM}}(H \leq u \mid X = \mathbf{x})) = \underbrace{a(u) + \langle \mathbf{b}(u), \mathbf{x} \rangle}_{=: f_u(\mathbf{x})}, \quad (u \in \mathcal{U} = [1, J]). \quad (7)$$

Continuous functions $a : \mathcal{U} \rightarrow \mathbb{R}$, $\mathbf{b} : \mathcal{U} \rightarrow \mathbb{R}^d$, and their weak derivatives $a^{[1]}$, $\mathbf{b}^{[1]}$, are defined later in (9)–(12); we use the weak derivative $f_u^{[1]}(\mathbf{x}) := a^{[1]}(u) + \langle \mathbf{b}^{[1]}(u), \mathbf{x} \rangle$ to obtain the conditional probability density (CPD) of $H \mid X$ as

$$q(u \mid X = \mathbf{x}) = \nabla_u \mathbb{P}_{\text{N}^3\text{POM}}(H \leq u \mid X = \mathbf{x}) = \sigma^{[1]}(f_u(\mathbf{x})) f_u^{[1]}(\mathbf{x}). \quad (8)$$

$\sigma(z) = 1/(1 + \exp(-z))$ denotes a sigmoid function and $\sigma^{[1]}$ is its derivative. To prevent a non-negative probability density, the prediction model $f_u(\mathbf{x})$ should be non-decreasing (with respect to $u \in \mathcal{U}$, for any fixed $\mathbf{x} \in \mathcal{X}$). Accordingly, we show a sufficient condition to guarantee the monotonicity in Section 3.2 and provide a parameter estimation algorithm in Section 3.3. Furthermore, in Section 3.4, we consider training N³POM even if only the discrete response is available. Note that estimating the CCP $\mathbb{P}_{\text{N}^3\text{POM}}(H \leq u \mid X = \mathbf{x}) = \sigma(f_u(\mathbf{x}))$ is equivalent to estimating $\mathbb{P}_{\text{N}^3\text{POM}}(H > u \mid X = \mathbf{x}) = 1 - \mathbb{P}_{\text{N}^3\text{POM}}(H \leq u \mid X = \mathbf{x}) = 1 - \sigma(f_u(\mathbf{x})) = \sigma(-f_u(\mathbf{x}))$.

To fully define the N³POM, we define the parametric functions a , \mathbf{b} and their weak derivatives $a^{[1]}$, $\mathbf{b}^{[1]}$, in the remaining part of this section.

- Regarding the function $a : \mathcal{U} \rightarrow \mathbb{R}$, this study considers a piece-wise linear functions with user-specified $R \in \mathbb{N}$ and $1 = j_1 < j_2 < \dots < j_R = J$ (such that $\mathcal{U} = [j_1, j_R]$):

$$a(u) := \begin{cases} \alpha_r & (u = j_r, r \in \{1, 2, \dots, R\}) \\ \alpha_{r-1} + s_{r-1}(u - j_{r-1}) & (u \in (j_{r-1}, j_r), r \in \{2, 3, \dots, R\}) \end{cases}, \quad (9)$$

where $s_{r-1} := \frac{\alpha_r - \alpha_{r-1}}{j_r - j_{r-1}}$ denotes the slope of the line connecting two points (j_{r-1}, α_{r-1}) and (j_r, α_r) . $-\infty < \alpha_1 \leq \alpha_2 \leq \dots \leq \alpha_R < \infty$ are parameters to be estimated. This piece-wise linear function is non-decreasing and satisfying $a(j_r) = \alpha_r$ ($r \in \{1, 2, \dots, R\}$). Consider a disjoint division of the interval \mathcal{U} :

$$\mathcal{U}_{r-1} := \begin{cases} [j_{r-1}, j_r) & (r \in \{2, 3, \dots, R-1\}) \\ [j_{R-1}, j_R] & (r = R) \end{cases} \quad \text{satisfying} \quad \bigcup_{r=2}^R \mathcal{U}_{r-1} = \mathcal{U}, \mathcal{U}_r \cap \mathcal{U}_{r'} = \emptyset \ (r \neq r').$$

Then, we obtain the following weak derivative:

$$a^{[1]}(u) := \sum_{r=2}^R \mathbb{1}(u \in \mathcal{U}_{r-1}) s_{r-1}. \quad (10)$$

- Regarding the vector-valued function $\mathbf{b}(u) = (b_1(u), b_2(u), \dots, b_d(u)) : \mathcal{U} \rightarrow \mathbb{R}^d$, we employ independent neural networks (NNs) $b_1, b_2, \dots, b_d : \mathcal{U} \rightarrow \mathbb{R}$ defined by

$$b_k(u) := v_k^{(2)} + \sum_{\ell=1}^L w_{k,\ell}^{(2)} \rho(w_{k,\ell}^{(1)} u + v_{k,\ell}^{(1)}), \quad (k \in \{1, 2, \dots, d\}), \quad (11)$$

where $\boldsymbol{\psi}_k := \{w_{k,\ell}^{(2)}, w_{k,\ell}^{(1)}, v_k^{(2)}, v_{k,\ell}^{(1)}\}_\ell$ is a set of weights to be estimated. As is well-known, the neural network $\mathbf{b}(u)$ has a universal approximation capability, that is, $\mathbf{b}(u)$ is capable of approximating any continuous function $\mathbf{b}_*(u)$ by increasing the number of hidden units $L \rightarrow \infty$ (see, e.g., [Cybenko \(1989\)](#)). $\rho : \mathbb{R} \rightarrow \mathbb{R}$ denotes an activation function. Generally, we assume that

$$(i) \ \rho \text{ is twice-differentiable, and } (ii) \ \rho_\infty^{[1]} := \sup_{z \in \mathbb{R}} |\rho(z)'| < \infty.$$

The sigmoid function $\rho(z) = 1/(1 + \exp(-z))$ and hyperbolic tangent function $\rho(z) = \tanh(z) := \{\exp(z) - \exp(-z)\}/\{\exp(z) + \exp(-z)\}$ satisfy conditions (i) and (ii). Note that $b_k(u)$ reduces to a constant $v_k^{(2)}$ (which is independent of u) if $w_{k,\ell}^{(2)} = 0$ for all ℓ . Each entry of the derivative $\mathbf{b}^{[1]}(u) = (b_1^{[1]}(u), b_2^{[1]}(u), \dots, b_d^{[1]}(u))$ of the NN $\mathbf{b}(u)$ is

$$b_k^{[1]}(u) := \sum_{\ell=1}^L w_{k,\ell}^{(1)} w_{k,\ell}^{(2)} \rho^{[1]}(w_{k,\ell}^{(1)} u + v_{k,\ell}^{(1)}), \quad (k \in \{1, 2, \dots, d\}). \quad (12)$$

3.2 Monotonicity of N³POM

Given that the CCP $\mathbb{P}(H \leq u \mid X = \mathbf{x})$ should be non-decreasing with respect to $u \in \mathcal{U}$ (for any fixed $\mathbf{x} \in \mathcal{X}$), we consider the monotonicity of the N³POM (7). Equivalently, we focus on the monotonicity of the prediction model $f_u(\mathbf{x}) = a_u(\mathbf{x}) + \langle \mathbf{b}(u), \mathbf{x} \rangle$.

First, we consider the function $a(u)$. Given that $f_u(\mathbf{0}) = a(u) + \langle \mathbf{b}(u), \mathbf{0} \rangle = a(u)$ should be monotone with respect to u , parameters in the function $a(u)$ should satisfy the inequality

$$\alpha_1 \leq \alpha_2 \leq \dots \leq \alpha_R; \quad (13)$$

we employ a re-parameterization

$$\alpha_r = \alpha_r(\boldsymbol{\varphi}) = \begin{cases} \phi & (r = 1) \\ \phi + \sum_{t=2}^r |\varphi_t| & (r = 2, 3, \dots, R) \end{cases}, \quad (14)$$

equipped with newly-defined parameters $\boldsymbol{\varphi} = (\phi, \varphi_2, \varphi_3, \dots, \varphi_R) \in \mathbb{R}^R$ to be estimated. By virtue of the aforementioned re-parameterization, the monotonicity inequality (13) always holds.

Second, we consider the function $\mathbf{b}(u)$. We focus on the type of function $\mathbf{b}(u)$, which can satisfy the monotonicity constraint of the CCP. Unfortunately, we find that the function $\mathbf{b}(u)$ is limited to constant functions, if the N³POM is monotone for all the covariates in the unbounded region, that is, the entire Euclidean space \mathbb{R}^d . See Proposition 1 with the proof shown in Appendix C.

Proposition 1. Let $a : \mathcal{U} \rightarrow \mathbb{R}$ be a function defined in (9), equipped with the re-parameterization (14). Let $\mathbf{b} : \mathcal{U} \rightarrow \mathbb{R}^d$ be a continuous function. If $f_u(\mathbf{x}) := a(u) + \langle \mathbf{b}(u), \mathbf{x} \rangle$ is non-decreasing with respect to $u \in \mathcal{U}$ for any fixed $\mathbf{x} \in \mathbb{R}^d$, $\mathbf{b}(u)$ is a constant function.

While N³POM cannot be uniformly monotone over the entire covariate Euclidean space, covariates are usually expected to distribute in a specific bounded region. Therefore, instead of the unbounded Euclidean space \mathbb{R}^d , we consider a closed ball region (i.e., a bounded region) for \mathbf{x} :

$$\mathcal{X}_2(\eta) := \{\mathbf{x} \in \mathbb{R}^d \mid \|\mathbf{x}\|_2 \leq \eta\}$$

equipped with a user-specified parameter $\eta > 0$, and we prove that N³POM can be monotone for all $\mathbf{x} \in \mathcal{X}_2(\eta)$. A sufficient condition provided for proving the monotonicity is satisfying an inequality

$$\min_{r=2,3,\dots,R} s_{r-1} \geq \eta \cdot \rho_\infty^{[1]} \cdot \sqrt{\sum_{k=1}^d \left\{ \sum_{\ell=1}^L |w_{k,\ell}^{(2)} w_{k,\ell}^{(1)}| \right\}^2}, \quad (15)$$

with $\rho_\infty^{[1]} := \max_{z \in \mathbb{R}} |\rho^{[1]}(z)|$. For instance, $\rho_\infty^{[1]} = 1/4$ for the sigmoid function $\rho(z) = 1/(1 + \exp(-z))$, and $\rho_\infty^{[1]} = 1$ for $\rho(z) = \tanh(z)$. $s_{r-1} := \{a_r - a_{r-1}\} / \{j_r - j_{r-1}\} = \varphi_r^2 / \{j_r - j_{r-1}\}$ represents a slope of the function $a(u)$. Then, the following proposition holds, with the proof given in Appendix C. See Figure 2 for illustration.

Proposition 2. Let $a : \mathcal{U} \rightarrow \mathbb{R}$ be a function defined in (9), equipped with the re-parameterization (14). Let $\mathbf{b} : \mathcal{U} \rightarrow \mathbb{R}^d$ be a neural network defined in (11) for each. Suppose the inequality (15) holds. Then, $f_u(\mathbf{x})$ is non-decreasing with respect to $u \in \mathcal{U}$, for any fixed $\mathbf{x} \in \mathcal{X}_2(\eta)$.

Therefore, by specifying $\eta > \max_i \|\mathbf{x}_i\|_2$, the estimated CCPs for all observed covariates $\{\mathbf{x}_i\}_{i=1}^n$ satisfy the monotonicity as $\{\mathbf{x}_i\}_{i=1}^n \subset \mathcal{X}_2(\eta)$.

Here, we consider the relation to Proposition 1. Substituting $\eta = \infty$ (corresponding to $\mathcal{X}_2(\eta) = \mathbb{R}^d$) into the inequality (15) yields the identity $\max_{k,\ell} |w_{k,\ell}^{(2)} w_{k,\ell}^{(1)}| = 0$. Namely, $w_{k,\ell}^{(2)} = 0$ or $w_{k,\ell}^{(1)} = 0$ for all k, ℓ ; the function $b_k(u)$ then reduces to a constant function $b_k(u) = \sum_{\ell=1}^L w_{k,\ell}^{(2)} \rho(v_{k,\ell}^{(1)}) + v_{k,\ell}^{(2)}$, which is also indicated in Proposition 1. Conversely, specifying small η allows larger fluctuation of $\mathbf{b}(u)$ because the neural network weights $\{w_{k,\ell}^{(2)}, w_{k,\ell}^{(1)}\}$ can take larger values in terms of absolute value. Therefore, there exists a trade-off between the model flexibility and the area of the covariate region in which the CCP is monotone.

The unfavorable property highlighted in Proposition 1 also holds for conventional NPOM approaches; however, to the best of our knowledge, none of the existing studies have explicitly mentioned this Proposition. Regarding the existing approaches relevant to Tutz and Berger (2022), Lu et al. (2022), and Wurm et al. (2021), which penalize the distance between the coefficients and the prototype $\|\boldsymbol{\beta}_j - \boldsymbol{\beta}_*\|$, increasing the penalty weight corresponds to decreasing η in our approach. Although they have attempted to specify the penalty weights so that the CCP preserves the monotonicity over the observed covariates in the training dataset, they are not guaranteed to be monotone in the out-of-sample region.

3.3 Monotonicity-preserving stochastic (MPS) algorithm

Using the CPD $q(u \mid X = \mathbf{x})$ defined in (8), we propose an *monotonicity-preserving stochastic* (MPS) algorithm. An MPS algorithm estimates the parameters of the prediction model $f_u(\mathbf{x}) = a(u) + \langle \mathbf{b}(u), \mathbf{x} \rangle$ by

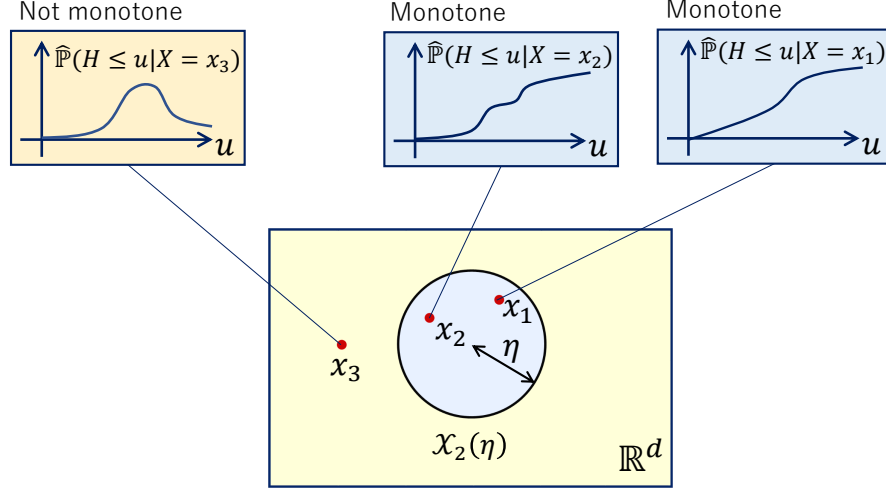


Figure 2: Illustration of Proposition 2. The estimated CCP $\hat{\mathbb{P}}_{\text{N}^3\text{POM}}(H \leq u \mid X = \mathbf{x}) = \sigma(\hat{f}_u(\mathbf{x}))$ is non-decreasing with respect to $u \in \mathcal{U}$ (i.e., valid) if $\mathbf{x} \in \mathcal{X}_2(\eta)$, while monotonicity is not guaranteed (i.e., invalid) if $\mathbf{x} \notin \mathcal{X}_2(\eta)$.

greedily maximizing the weighted log-likelihood as follows:

$$\begin{aligned} \ell_{\zeta}(\boldsymbol{\theta}) &:= \sum_{i=1}^n \zeta_i \log q(h_i \mid X = \mathbf{x}_i) \\ &= \sum_{i=1}^n \zeta_i \{ \log \sigma^{[1]}(a(h_i) + \langle \mathbf{b}(h_i), \mathbf{x}_i \rangle) + \log(a^{[1]}(h_i) + \langle \mathbf{b}^{[1]}(h_i), \mathbf{x}_i \rangle) \}, \end{aligned} \quad (16)$$

under the sufficient condition constraint (15). $\zeta_i \geq 0$ ($i \in \{1, 2, \dots, n\}$) are user-specified weights satisfying $\sum_{i=1}^n \zeta_i = 1$ (e.g., $\zeta_1 = \zeta_2 = \dots = \zeta_n = 1/n$). (16) is a continuous variant of the log-likelihood used in conventional NPOM. See Remark 1.

With an initial parameter $\boldsymbol{\theta}^{(0)}$, the MPS algorithm iteratively repeats the following two steps for $t = 1, 2, \dots$ until convergence.

- (i) Compute a single step of the mini-batch gradient ascent algorithm (Goodfellow et al., 2016) regarding the parameters $\boldsymbol{\varphi} = (\varphi_1, \varphi_2, \dots, \varphi_R)$ for $a(u)$ and $\boldsymbol{\psi} = \{w_{k,\ell}^{(2)}, w_{k,\ell}^{(1)}, v_k^{(2)}, v_{k,\ell}^{(1)}\}_{k,\ell}$ for $\mathbf{b}(u)$. Explicit forms of the gradients for the gradient ascent are shown in Appendix A.

- (ii) With the coefficient

$$c = \min \left\{ 1, \frac{\min_{r=2,3,\dots,R} S_{r-1}}{\eta \cdot \rho_{\infty}^{[1]} \cdot \sqrt{\sum_{k=1}^d \left\{ \sum_{\ell=1}^L |w_{k,\ell}^{(2)} w_{k,\ell}^{(1)}|^2 \right\}}} \right\},$$

we replace $w_{k,\ell}^{(2)}, w_{k,\ell}^{(1)}$ by $\sqrt{c} \cdot w_{k,\ell}^{(2)}, \sqrt{c} \cdot w_{k,\ell}^{(1)}$ so as to satisfy the inequality (15), that is a sufficient condition to guarantee the monotonicity of the predicted CCP.

Different from the standard mini-batch gradient ascent algorithm (consisting of only step (i)), step (ii) is needed to guarantee the monotonicity of the predicted CCP $\hat{\mathbb{P}}_{\text{N}^3\text{POM}}(H \leq u \mid X = \mathbf{x})$, as discussed in Section 3.2.

Remark 1 (Relation to the likelihood of NPOM). Define a function $v_i(\Delta) = \{\mathbb{P}(H \leq h_i \mid X = \mathbf{x}_i) - \mathbb{P}(H \leq h_i - \Delta \mid X = \mathbf{x}_i)\} / \Delta$ (satisfying $\lim_{\Delta \searrow 0} v_i(\Delta) = q(h_i \mid X = \mathbf{x}_i)$) and $j_1 = 1, j_2 = 2, \dots, j_R = R = J$. Accordingly,

the log-likelihood (16) corresponds to $\sum_{i=1}^n \zeta_i \log\{\lim_{\Delta \searrow 0} \nu_i(\Delta)\}$ while the log-likelihood of the discrete NPOM is its discrete approximation $\sum_{i=1}^n \zeta_i \log \nu_i(1)$ (see, e.g., Peterson and Harrell (1990)).

3.4 Adaptation to the discrete responses

While we consider the response $H \in [1, J]$ taking a value in the connected interval $[1, J]$, it would be worthwhile to consider the adaptation to the discrete response $G \in \{1, 2, \dots, J\}$ because of the variety of applications. Although the proposed N³POM (7) can be formally trained using the discrete response, the discrete responses are not sufficient to fully train the continuous model $f_u(\mathbf{x})$. Experimentally, using several synthetic and real-world datasets, N³POM trained using discrete response behaves similarly to the POM model (i.e., the estimated coefficients $\mathbf{b}(u)$ reduce to a constant) even if the underlying function is response-dependent. To address this issue, we propose incorporating an additive perturbation to the responses so that the responses take values in not only $\{1, 2, \dots, J\}$ but also the connected interval $[1, J]$.

Our idea is simple. If we have the discrete responses $g_1, g_2, \dots, g_n \in \{1, 2, \dots, J\}$, we can uniformly generate the random numbers e_1, e_2, \dots, e_n i.i.d. over the region $[-0.5, 0.5]$ and add e_1, e_2, \dots, e_n to g_1, g_2, \dots, g_n , respectively. Finally, we round the obtained responses to take the values between 1 and J . Namely, we define a (random) perturbation operator

$$\mathfrak{C}(g_i) := \underset{j \in [1, J]}{\operatorname{argmin}} |(g_i + e_i) - j|, \quad (i \in \{1, 2, \dots, n\}). \quad (17)$$

Although heuristic, this perturbation operator (17) is explainable in the context of ordinary least squares regression. As is well-known in asymptotic theory, the estimated regression function in ordinary least squares converges to the conditional expectation $f_*(X) = \mathbb{E}[G | X]$; so adding the mean-zero perturbation, $E \sim U[-0.5, 0.5]$ is expected not to cause any bias (i.e., $\mathbb{E}[G + E | X] = \mathbb{E}[G | X] = f_*(X)$). A similar result is expected to hold for ordinal regression. While the estimation efficiency slightly decreases because of this perturbation, it is advantageous to fully train the continuous NN; see the numerical experiments in Section 4 for the effectiveness of the additive perturbation (17).

4 Experiments on Synthetic Datasets

This section provides numerical experiments using synthetic datasets.

4.1 Synthetic datasets

In this experiment, we set $n = 1000, d = 2, J = 7$. For the covariate X , we employ two different settings, (i) and (ii): (i) we generate $r_1, r_2, \dots, r_n \sim U([0, 1])$ and $\theta_1, \theta_2, \dots, \theta_n \sim U([0, 2\pi])$ uniformly and randomly, and compute $\mathbf{x}_i = (x_{ij}) = (r_i \cos \theta_i, r_i \sin \theta_i) \in \mathbb{R}^2$, (ii) we generate $x_{ij} \sim \text{Beta}(0.5, 0.5)$ ($j = 1, 2$) i.i.d. uniformly and randomly. $\text{Beta}(t_1, t_2)$ denotes Beta distribution, whose density is proportional to $x^{t_1-1}(1-x)^{t_2-1}$. We consider the functions $a_*(u) = 2u - 9$ and

$$\mathbf{b}_*(u) = (b_{*1}(u), b_{*2}(u)) = (-1 + m_1 u^2, 1 + m_2 u^2)$$

so that the continuous responses h_1, h_2, \dots, h_n are generated based on conditional distribution $\mathbb{P}(H \leq h_i | X = \mathbf{x}_i) = \sigma(a_*(h_i) + \langle \mathbf{b}_*(h_i), \mathbf{x}_i \rangle)$. We further truncate u to take the values in the interval $\mathcal{U} = [1, J]$ (by the function $\operatorname{argmin}_{\tilde{u} \in [1, J]} \|u - \tilde{u}\|$), with $J = 7$. (Note that the randomly generated u rarely breaches the interval $[1, 7]$ in this setting). The observed covariates $\mathbf{x}_1, \mathbf{x}_2, \dots, \mathbf{x}_n$ lie in the unit disk $\mathcal{X}_2(1) = \{\mathbf{x} \in \mathbb{R}^2 | \|\mathbf{x}\|_2 \leq 1\}$; the underlying function $f_u(\mathbf{x}) = a_*(u) + \langle \mathbf{b}_*(u), \mathbf{x} \rangle$ is non-decreasing with respect to $u \in \mathcal{U}$ for all $\mathbf{x} \in \mathcal{X}_2(1)$, as $f_u^{[1]}(\mathbf{x}) = \nabla_u f_u(\mathbf{x}) = 2 - 2m_1 u x_1 + 2m_2 u x_2 \geq 0$.

To compute the baselines, we discretize the observed continuous responses h_i as

$$[h_i] := \underset{j \in \{1, 2, \dots, J\}}{\operatorname{argmin}} \|h_i - j\|_2; \quad (18)$$

Table 1: Results of the MSE experiments on synthetic datasets, where the observed covariates are generated by the setting (i) $x_i = (r_i \cos \theta_i, r_i \sin \theta_i)$, $r_i \sim U([0, 1])$, $\theta_i \sim U([0, 2\pi])$. For the 20 experiments for each setting, the median and standard deviation (shown in parenthesis) are computed. The best score is **bolded and blue-colored**, while the second best score is **bolded and red-colored**

(a) Both coefficients $b_{*1}(u) = -1 + m_1 u^2$, $b_{*2}(u) = 1 + m_2 u^2$ are response-dependent (i.e., not constant).

| Model | Optimizer | Response | $(m_1, m_2) = (0.05, -0.05)$ | | $(m_1, m_2) = (0.05, 0.05)$ | |
|--------------------|----------------|-----------------------|------------------------------|----------------------|-----------------------------|----------------------|
| | | | MSE(\hat{b}_1) | MSE(\hat{b}_2) | MSE(\hat{b}_1) | MSE(\hat{b}_2) |
| N ³ POM | MPS | h_i | 0.066 (0.155) | 0.122 (0.147) | 0.052 (0.062) | 0.134 (0.138) |
| N ³ POM | MPS | $\mathfrak{C}([h_i])$ | 0.116 (0.060) | 0.163 (0.081) | 0.084 (0.098) | 0.177 (0.117) |
| N ³ POM | MPS | $[h_i]$ | 0.516 (0.044) | 0.527 (0.020) | 0.530 (0.040) | 0.525 (0.040) |
| POM | polr | $[h_i]$ | 0.516 (0.026) | 0.514 (0.017) | 0.514 (0.030) | 0.524 (0.034) |
| NPOM | (ridge) oNet | $[h_i]$ | 0.233 (0.037) | 0.265 (0.073) | 0.356 (0.030) | 2.572 (0.169) |
| NPOM | (elastic) oNet | $[h_i]$ | 0.243 (0.170) | 0.270 (0.166) | 0.215 (0.070) | 0.229 (0.101) |
| NPOM | (lasso) oNet | $[h_i]$ | 0.209 (0.151) | 0.266 (0.173) | 0.237 (0.085) | 0.223 (0.105) |
| NPOM [†] | (ridge) oNet | $[h_i]$ | 0.253 (0.055) | 0.270 (0.070) | 0.418 (0.023) | 1.129 (0.080) |
| NPOM [†] | (elastic) oNet | $[h_i]$ | 0.262 (0.161) | 0.274 (0.144) | 0.198 (0.093) | 0.209 (0.089) |
| NPOM [†] | (lasso) oNet | $[h_i]$ | 0.261 (0.153) | 0.265 (0.179) | 0.206 (0.097) | 0.243 (0.120) |
| NPOM | serp | $[h_i]$ | 0.174 (0.066) | 0.204 (0.079) | 0.130 (0.074) | 0.186 (0.074) |

(b) At least one of $b_{*1}(u) = -1 + m_1 u^2$, $b_{*2}(u) = 1 + m_2 u^2$ is a constant function, that is, either $m_1 = 0$ or $m_2 = 0$.

| Model | Optimizer | Response | $(m_1, m_2) = (0.05, 0)$ | | $(m_1, m_2) = (0, 0)$ | |
|--------------------|----------------|-----------------------|--------------------------|----------------------|-----------------------|----------------------|
| | | | MSE(\hat{b}_1) | MSE(\hat{b}_2) | MSE(\hat{b}_1) | MSE(\hat{b}_2) |
| N ³ POM | MPS | h_i | 0.083 (0.164) | 0.075 (0.048) | 0.046 (0.034) | 0.052 (0.060) |
| N ³ POM | MPS | $\mathfrak{C}([h_i])$ | 0.110 (0.129) | 0.041 (0.042) | 0.035 (0.048) | 0.036 (0.059) |
| N ³ POM | MPS | $[h_i]$ | 0.526 (0.037) | 0.007 (0.020) | 0.004 (0.016) | 0.011 (0.019) |
| POM | polr | $[h_i]$ | 0.513 (0.029) | 0.002 (0.023) | 0.008 (0.018) | 0.002 (0.019) |
| NPOM | (ridge) oNet | $[h_i]$ | 0.310 (0.053) | 0.533 (0.063) | 0.559 (0.044) | 0.561 (0.044) |
| NPOM | (elastic) oNet | $[h_i]$ | 0.221 (0.081) | 0.178 (0.145) | 0.286 (0.124) | 0.192 (0.131) |
| NPOM | (lasso) oNet | $[h_i]$ | 0.211 (0.098) | 0.198 (0.161) | 0.321 (0.127) | 0.228 (0.129) |
| NPOM [†] | (ridge) oNet | $[h_i]$ | 0.388 (0.034) | 0.117 (0.034) | 0.121 (0.037) | 0.125 (0.039) |
| NPOM [†] | (elastic) oNet | $[h_i]$ | 0.391 (0.153) | 0.022 (0.057) | 0.013 (0.033) | 0.028 (0.022) |
| NPOM [†] | (lasso) oNet | $[h_i]$ | 0.277 (0.155) | 0.034 (0.032) | 0.011 (0.034) | 0.028 (0.040) |
| NPOM | serp | $[h_i]$ | 0.186 (0.077) | 0.027 (0.033) | 0.011 (0.019) | 0.020 (0.037) |

We train the POM and NPOM by leveraging $[h_i]$. Furthermore, we train the proposed N³POM with h_i , $[h_i]$ and $\mathfrak{C}([h_i])$ for comparison, where $\mathfrak{C}(\cdot)$ is the random perturbation operator defined in (17).

4.2 Experimental settings

Model architecture: We employ the proposed N³POM (7) defined in Section 3.1. We specify $R = 24$ for the function $a(u)$ and employ the regular intervals $1 = j_1 < j_2 < j_3 < \dots < j_{24} = 7$. The number of hidden units in the neural network $\mathbf{b}(u)$ is $L = 50$. The sigmoid activation function $\rho(z) = 1/(1 + \exp(-z))$ is also employed.

Initialization: First, we compute the coefficient vectors $\hat{\beta}_1, \hat{\beta}_2, \dots, \hat{\beta}_{J-1}$ of the discrete NPOM by leveraging `serp` package in R language. Next, we initialize the neural network parameters so that the NN outputs approximate the `serp` outputs over the discrete points (i.e., $b_k(j) \approx \hat{\beta}_{jk}$). See Appendix B for details. The

Table 2: Results of the MSE experiments on synthetic datasets, where the observed covariates are generated by the setting (ii) $x_{ij} \sim \text{Beta}(0.5, 0.5)$. Among the 20 experiments for each setting, the median and standard deviation (shown in parenthesis) are computed. The best score is **bolded and blue-colored**, while the second best score is **bolded and red-colored**

(a) Both coefficients $b_{*1}(u) = -1 + m_1 u^2$, $b_{*2}(u) = 1 + m_2 u^2$ are response-dependent (i.e., not constant).

| Model | Optimizer | Response | $(m_1, m_2) = (0.05, -0.05)$ | | $(m_1, m_2) = (0.05, 0.05)$ | |
|--------------------|----------------|-----------------------|------------------------------|----------------------|-----------------------------|----------------------|
| | | | MSE(\hat{b}_1) | MSE(\hat{b}_2) | MSE(\hat{b}_1) | MSE(\hat{b}_2) |
| N ³ POM | MPS | h_i | 0.179 (0.143) | 0.265 (0.206) | 0.200 (0.092) | 0.300 (0.202) |
| N ³ POM | MPS | $[h_i]$ | 0.250 (0.135) | 0.297 (0.148) | 0.186 (0.112) | 0.305 (0.164) |
| N ³ POM | MPS | $\mathfrak{C}([h_i])$ | 0.559 (0.055) | 0.599 (0.069) | 0.524 (0.024) | 0.563 (0.049) |
| POM | polr | $[h_i]$ | 0.522 (0.033) | 0.549 (0.045) | 0.521 (0.034) | 0.553 (0.037) |
| NPOM | (ridge) oNet | $[h_i]$ | 0.251 (0.070) | 0.278 (0.049) | 0.414 (0.043) | 3.239 (0.075) |
| NPOM | (elastic) oNet | $[h_i]$ | 0.481 (0.182) | 0.461 (0.187) | 0.350 (0.242) | 1.386 (0.780) |
| NPOM | (lasso) oNet | $[h_i]$ | 0.482 (0.255) | 0.439 (0.219) | 0.416 (0.418) | 1.502 (0.906) |
| NPOM [†] | (ridge) oNet | $[h_i]$ | 0.284 (0.085) | 0.318 (0.084) | 0.450 (0.026) | 1.456 (0.104) |
| NPOM [†] | (elastic) oNet | $[h_i]$ | 0.477 (0.148) | 0.364 (0.155) | 0.443 (0.12) | 0.571 (0.081) |
| NPOM [†] | (lasso) oNet | $[h_i]$ | 0.497 (0.253) | 0.419 (0.223) | 0.451 (0.293) | 0.552 (0.094) |
| NPOM | serp | $[h_i]$ | 0.207 (0.098) | 0.213 (0.078) | 0.277 (0.111) | 0.319 (0.118) |

(b) At least one of $b_{*1}(u) = -1 + m_1 u^2$, $b_{*2}(u) = 1 + m_2 u^2$ is a constant function, that is, either $m_1 = 0$ or $m_2 = 0$.

| Model | Optimizer | Response | $(m_1, m_2) = (0.05, 0)$ | | $(m_1, m_2) = (0, 0)$ | |
|--------------------|----------------|-----------------------|--------------------------|----------------------|-----------------------|----------------------|
| | | | MSE(\hat{b}_1) | MSE(\hat{b}_2) | MSE(\hat{b}_1) | MSE(\hat{b}_2) |
| N ³ POM | MPS | h_i | 0.195 (0.161) | 0.036 (0.099) | 0.050 (0.082) | 0.067 (0.117) |
| N ³ POM | MPS | $[h_i]$ | 0.293 (0.132) | 0.055 (0.051) | 0.056 (0.034) | 0.045 (0.052) |
| N ³ POM | MPS | $\mathfrak{C}([h_i])$ | 0.518 (0.043) | 0.026 (0.041) | 0.040 (0.031) | 0.015 (0.056) |
| POM | polr | $[h_i]$ | 0.517 (0.020) | 0.021 (0.032) | 0.023 (0.021) | 0.016 (0.033) |
| NPOM | (ridge) oNet | $[h_i]$ | 0.384 (0.065) | 0.556 (0.068) | 0.507 (0.074) | 0.554 (0.079) |
| NPOM | (elastic) oNet | $[h_i]$ | 0.438 (0.200) | 0.387 (0.201) | 0.203 (0.153) | 0.183 (0.198) |
| NPOM | (lasso) oNet | $[h_i]$ | 0.482 (0.467) | 0.507 (0.361) | 0.169 (0.236) | 0.228 (0.203) |
| NPOM [†] | (ridge) oNet | $[h_i]$ | 0.409 (0.050) | 0.151 (0.059) | 0.087 (0.067) | 0.129 (0.064) |
| NPOM [†] | (elastic) oNet | $[h_i]$ | 0.482 (0.063) | 0.130 (0.123) | 0.037 (0.051) | 0.059 (0.064) |
| NPOM [†] | (lasso) oNet | $[h_i]$ | 0.472 (0.058) | 0.118 (0.181) | 0.040 (0.060) | 0.052 (0.069) |
| NPOM | serp | $[h_i]$ | 0.278 (0.119) | 0.054 (0.052) | 0.041 (0.037) | 0.046 (0.053) |

parameters of the function $a(u)$ are also parameterized by linear interpolation of serp outputs.

Optimization: We compute a mini-batch gradient ascent algorithm (Goodfellow et al., 2016) for maximizing the log-likelihood (16). The weights are specified as $w_i \propto 1/n_{r_i}^{0.5}$, where $n_r := |\{i : g_i \in \mathcal{U}_r\}|$ and $g_i \in \mathcal{U}_{r_i}$. A mini-batch of size 16 is uniformly and randomly selected from training samples (without replacement), and the number of iterations is 5000. The learning rate is multiplied by 0.95 for each 50 iteration. Based on these settings, we apply the MPS algorithm to the following three types of observed responses: $h_i, \mathfrak{C}([h_i]), [h_i]$.

Baselines: We employ the following two major implementations of ordinal regression: polr function (using a logistic model) in MASS package and ordinalNet (oNet) function (using only non-parallel terms, cumulative logit, and a hyperparameter $\alpha \in \{0, 0.5, 1\}$) in ordinalNet package (Wurm et al., 2021), in R language. We also employ serp function (using logit link and “penalize” slope option) in serp package (Ugba et al., 2021); polr, ordinalNet, serp are used to train POM, NPOM, and NPOM, respectively.

ordinalNet decomposes $\beta_j = \beta_* + \delta_j$, where β_* is a parallel term and $\{\delta_j\}$ are non-parallel terms; we compute NPOM with only the non-parallel term (without parallel term, denoted simply as NPOM) and NPOM with both parallel and non-parallel terms (denoted as NPOM[†]). Given that ordinalNet penalizes the coefficients as $\alpha \|\beta_*\|_1 + (1 - \alpha) \|\beta_*\|_2^2 + \sum_{j=1}^{J-1} \{\alpha \|\delta_j\|_1 + (1 - \alpha) \|\delta_j\|_2^2\}$, $\alpha = 0, 0.5$ and 1 represent the ridge, elastic, and lasso penalties, respectively. `serp` penalizes the adjacent coefficients $\|\beta_j - \beta_{j-1}\|_2^2$.

The aforementioned baselines are applied to the discretized observed responses $[h_i]$.

Evaluation: for each estimated coefficient $\hat{b}_k(u)$, we compute mean squared error (MSE):

$$\text{MSE}(\hat{b}_k) := \frac{1}{|\tilde{\mathcal{U}}|} \sum_{\tilde{u} \in \tilde{\mathcal{U}}} \{b_{*k}(\tilde{u}) - \hat{b}_k(\tilde{u})\}^2 \quad (k = 1, 2),$$

with $\tilde{\mathcal{U}} := \{1, 1.05, 1.1, 1.15, 1.2, \dots, J\}$. For evaluating the POM and discrete NPOM, we employ linear interpolation for computing $\hat{b}_k(u)$ for non-integer u . We compute the MSE for each of the 30 times experiments. For a robust estimation of the MSE, we compute their median for each setting. We also compute the standard deviation of MSE after removing the best and worst MSEs for each setting.

4.3 Results

Setting(i). Experimental results for the covariate setting (i) $\mathbf{x}_i = (r_i \cos \theta_i, r_i \sin \theta_i)$, $r_i \sim U([0, 1])$, $\theta_i \sim U([0, 2\pi))$ are summarized in Table 1. For the response-dependent coefficients shown in Table 1(a), for all the cases, the N³POM trained using the observed continuous response h_i shows the best scores. The N³POM applied to the discretized observed response $[h_i]$ shows scores that are nearly equal to `polr`. Even if the response is discretized, the score gets closer to that of the observed continuous response by leveraging the adaptation to the discrete responses shown in Section 3.4. The scores of the NPOM implemented by `serp` package follow the scores of the N³POM. `ordinalNet` demonstrates the subsequent scores.

We also evaluate the proposed method and baselines when either of the coefficients is a constant (i.e., $m_1 = 0$ or $m_2 = 0$) in Table 1(b). Similarly to the case of response-dependent coefficients, the N³POM trained using the discretized response demonstrates a similar score to that of POM using `polr` package (though we initialized the neural network using `serp` package). For the constant coefficients (corresponding to $m_1 = 0$ or $m_2 = 0$), the POM and N³POM trained using the discrete responses demonstrate the best and second-best scores. This is because the POM assumes the constant coefficients, which is why the estimation variance is significantly smaller than that of the more flexible models, NPOM and N³POM.

Setting (ii). Experimental results for the covariate setting (ii) $x_{ij} \sim \text{Beta}(0.5, 0.5)$ are summarized in Table 2. Overall, the tendency is the same as in setting (i); N³POM trained using the observed continuous response h_i demonstrates the best scores for estimating almost all non-constant coefficients. Moreover, the POM and N³POM trained using the discrete response $[h_i]$ demonstrate the best scores for estimating the constant coefficients.

5 Experiments on Real-World Datasets

In this section, we train N³POM by leveraging real-world datasets. We show and interpret the results of the experiments for `autoMPG6`, `autoMPG8`, and `real-estate` datasets and show the results of `boston-housing`, `concrete`, and `airfoil` datasets. We also describe the experimental settings.

5.1 Real-world datasets

We employ the following datasets collected from the UCI machine learning repository (Dua and Graff, 2017).

autoMPG6 ($n = 392, d = 5$) and **autoMPG8** ($n = 392, d = 7$). The autoMPG6 dataset consists of five covariates (“Displacement” (continuous), “Horse power” (continuous), “Weight” (continuous), “Acceleration” (continuous), “Model year” (discrete)), and continuous response “mpg”. “mpg” stands for miles per gallon, representing fuel efficiency. The autoMPG8 dataset is an extension of autoMPG6, where two additional covariates (“Cylinders” (discrete) and “Origin” (discrete)) are incorporated. The remaining five covariates and responses are the same as that of autoMPG6. Although these datasets are almost the same, we can examine whether the estimated coefficients are more robust compared with the newly additional covariates by comparing N³POM trained with these datasets.

real-estate ($n = 413, d = 3$). Among the six covariates in the original real-estate dataset, we employ the three covariates “X2:house age”, “X3:distance to the nearest MRT station”, and “X4:number of convenience stores”, and remove the following covariates: “X1:transaction date”, “X5:latitude”, and “X6:longitude”. They are renamed to “house age”, “Dist. to station”, and “Num. of conv. stores” in our experiments. The response variable represents the house price of the unit area. Thus, we rename this variable as “house price oua”. For meaningful computation, we remove the 271st column because its observed response is an outlier whose difference from the mean of the remaining responses is farther than six times the standard deviation.

For each dataset, observed covariates are standardized (centering and scaling). Responses are linearly transformed so that $\min_i h_i = 1, \max_i h_i = 10$ (i.e., we set $J = 10$). After computing N³POM, we recover the original response for plot by applying the inverse linear transformation. See Supplement D for N³POM applied to boston-housing ($n = 502, d = 12$), concrete ($n = 1030, d = 8$), and airfoil ($n = 1503, d = 5$) datasets, and Supplement E for pairwise scatter plots of the observed covariates in these datasets.

5.2 Experimental settings

Initialization and optimization are the same as the experiments in Section 4, while we employ $R = 20$ with equal intervals $1 = j_1 < j_2 < \dots < j_R = J = 10$ in real-world dataset experiments.

First, we compute the `serp` function by leveraging the rounded responses $[h_i]$. Initialized by this `serp` output (see Appendix B), we train the neural network by the MPS algorithm. For considering the randomness of choosing mini-batches, we compute 10 different stochastic optimization results in each plot. For comparison, we also plot the initial neural network (approximating the preliminarily computed `serp` output) and POM coefficients trained using the `polr` function.

5.3 Results

Estimated coefficients for each dataset are shown in Figures 3–6. For interpretation, we inverse the sign of the estimated coefficients $\hat{\mathbf{b}}(u)$ because we have a probability that the response exceeds the threshold value u as:

$$\text{logit}(\hat{\mathbb{P}}_{\text{N}^3\text{POM}}(H > u \mid X = \mathbf{x})) = \text{logit}(1 - \hat{\mathbb{P}}_{\text{N}^3\text{POM}}(H \leq u \mid X = \mathbf{x})) = \hat{r}(u) + \langle \hat{\mathbf{s}}(u), \mathbf{x} \rangle$$

with $\hat{r}(u) = -\hat{a}(u)$ and

$$\hat{\mathbf{s}}(u) = (\hat{s}_1(u), \hat{s}_2(u), \dots, \hat{s}_d(u)) = -\hat{\mathbf{b}}(u).$$

Therefore, the larger $\hat{s}_k(u) = -\hat{b}_k(u)$ (corresponding to smaller $\hat{b}_k(u)$) indicates a larger response if the corresponding observed covariate is large.

autoMPG6 and autoMPG8. First, we consider the results of autoMPG6 ($n = 392, d = 5$) and autoMPG8 ($n = 392, d = 7$) datasets shown in Figures 3 and 4, respectively. While the autoMPG8 dataset includes the additional two covariates, “Cylinders” and “Origin”, the tendency of the estimated coefficients $\hat{s}_k(u)$ of the 5 common covariates (“Displacement”, “Horse power”, “Weight”, “Acceleration”, and “Model year”) is almost the same for these two datasets. Regarding the 5 common covariates, The coefficients $\hat{s}_k(u)$ of “Displacement”, “Horse power”, and “Weight” are negative and decreasing. Hence, taking higher displacement (or horse power/weight) indicates lower fuel efficiency, which adversely affects the fuel efficiency in highly efficient cars. The remaining covariates $\hat{s}_k(u)$ for “Acceleration” and “Model year” are increasing, which indicates higher fuel efficiency and their importance also increases for highly efficient cars.

real-estate. The results of real-estate ($n = 413, d = 3$) dataset are shown in Figure 5(a). For the second covariate, “Dist. to station”, the increasing distance adversely affects the house price. Moreover, the degree of the adverse effect increases for more expensive houses. The third covariate, “Number of convenience stores” positively affects the house price. However, the degree of the positive effect decreases for more expensive houses. For the first covariate, “House age”, the age of the house adversely affects the house price for lower-price houses; however, this effect almost vanishes (as $\hat{s}_1(u)$ approaches 0 as u increases) for higher price houses. See Figure 5(b) for the scatter plots between covariates and house price. For instance, we can observe that the house age does not seem to adversely affect the house price for higher price houses, while it seems to have a slightly negative effect when considering lower-priced houses.

The regression results of several datasets are also provided in Supplement D. Additionally, see Supplement E for pairwise scatter plots of all datasets used in this study.

While the coefficients $\mathbf{s}(u) = -\mathbf{b}(u)$ considered in this study are expected to represent the influence of each covariate to the CCP, more strictly speaking, they in fact show the influence on the logit function applied to the CCP. Namely, the coefficients are also influenced by the logit function, and the coefficients in the tail region ($u \approx 0, u \approx J$) tend to be amplified; we may employ a marginal effect (Agresti and Tarantola, 2018) $\frac{\partial}{\partial \mathbf{x}} \mathbb{P}_{\text{N}^3\text{POM}}(H > u \mid X = \mathbf{x}) = \mathbf{s}(u) \sigma^{[1]}(-f_u(\mathbf{x}))$ when considering the influence on the CCP directly. However, the marginal effect differs depending on the covariate X and it tends to (excessively) shrink the influence to 0 in the tail region ($u \approx 0, u \approx J$) as $\sigma^{[1]}(-\infty) = \sigma^{[1]}(+\infty) = 0$; unlike the simple coefficients $\mathbf{s}(u)$, marginal effect cannot capture the tendency whether the influence of the covariate increases or decreases (as u increases), due to the shrinking behavior in the tail region. In the case of real-estate dataset above, the interesting coefficient $s_k(u)$ of house-age that approximates 0 as $u \approx J$, cannot be detected when using the marginal effect, as almost all marginal effects approximates 0 as $u \approx J$ (regardless of how the coefficient is important in the tail region). As a future work, it would be worthwhile to consider a more interpretable score to evaluate the influence of the covariates in the context of ordinal regression.

6 Conclusion

We proposed a continuous neural network-based non-proportional odds model (N³POM) for ordinal regression. In our model, we computed the linear coefficients of ordinal regression by the neural network, taking the ordinal and continuous response as its input. By virtue of the neural network, the estimated coefficients might have flexibility while preserving the interpretability of the conventional ordinal regression models. We showed a sufficient condition to preserve the monotonicity of the predicted conditional cumulative probabilities. We also provided an MPS algorithm to adequately train the neural network. The N³POM demonstrated better scores than the existing ones in synthetic dataset experiments. Thus, we trained the N³POM using several real-world datasets.

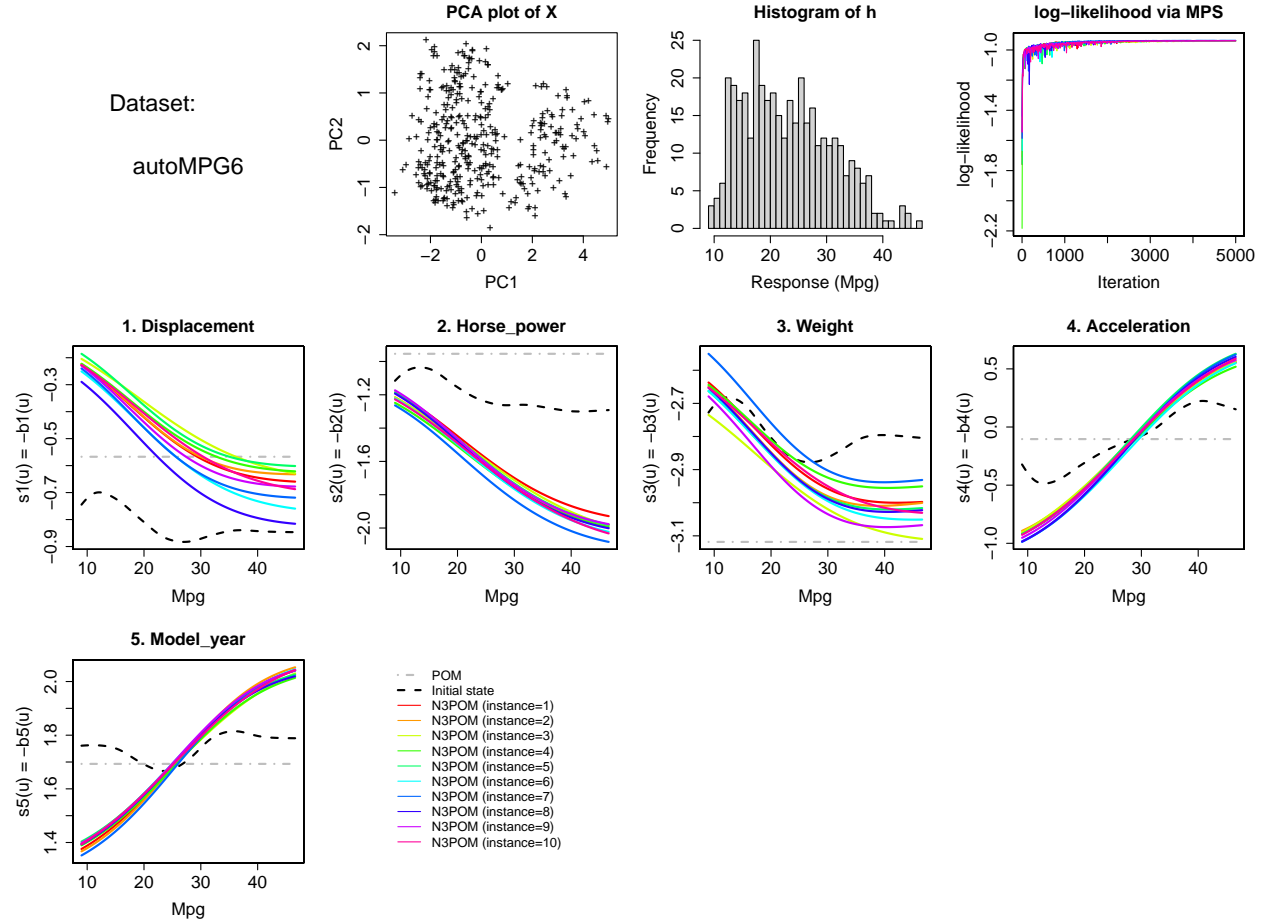


Figure 3: autoMPG6 dataset experiment.

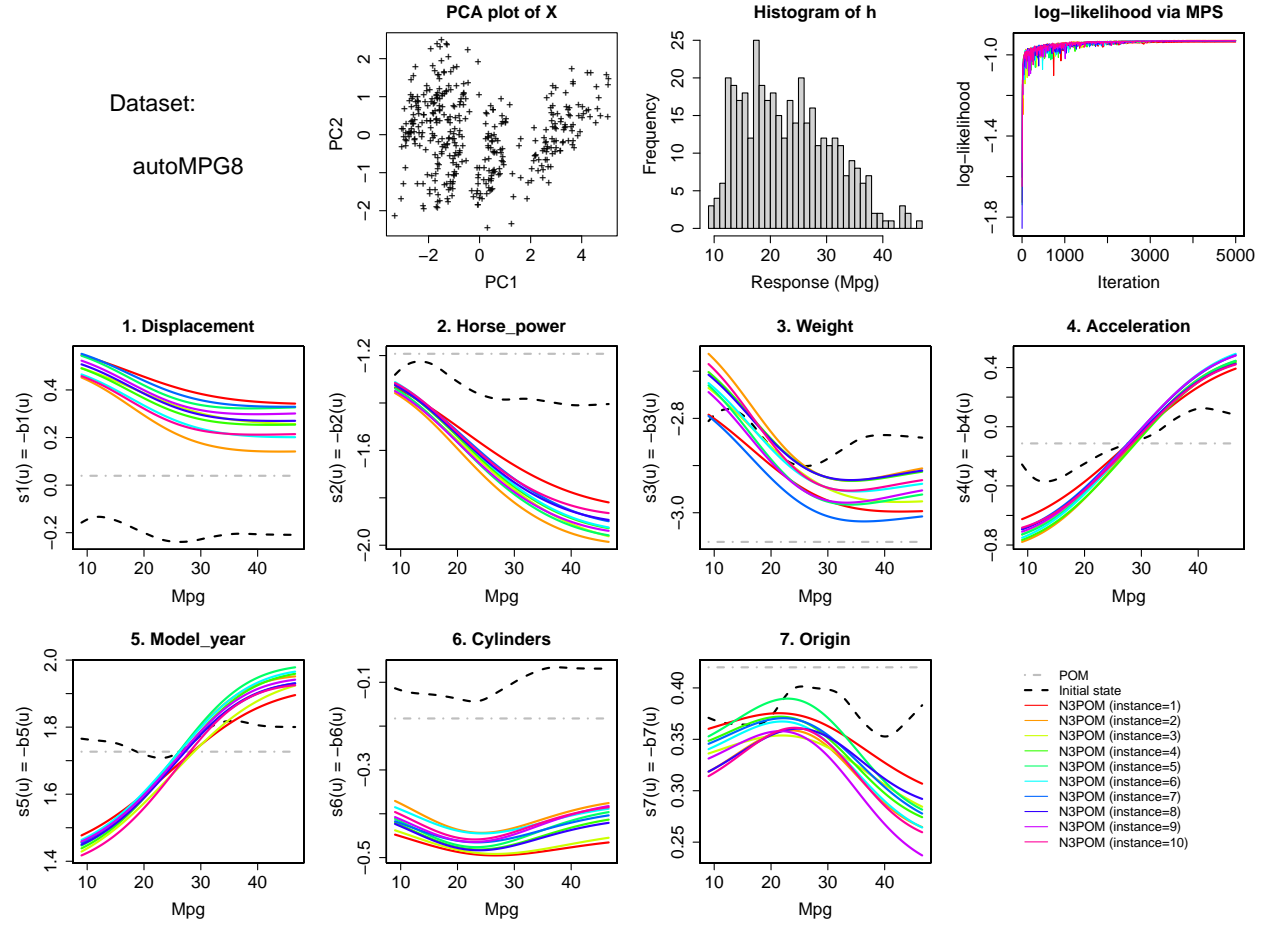
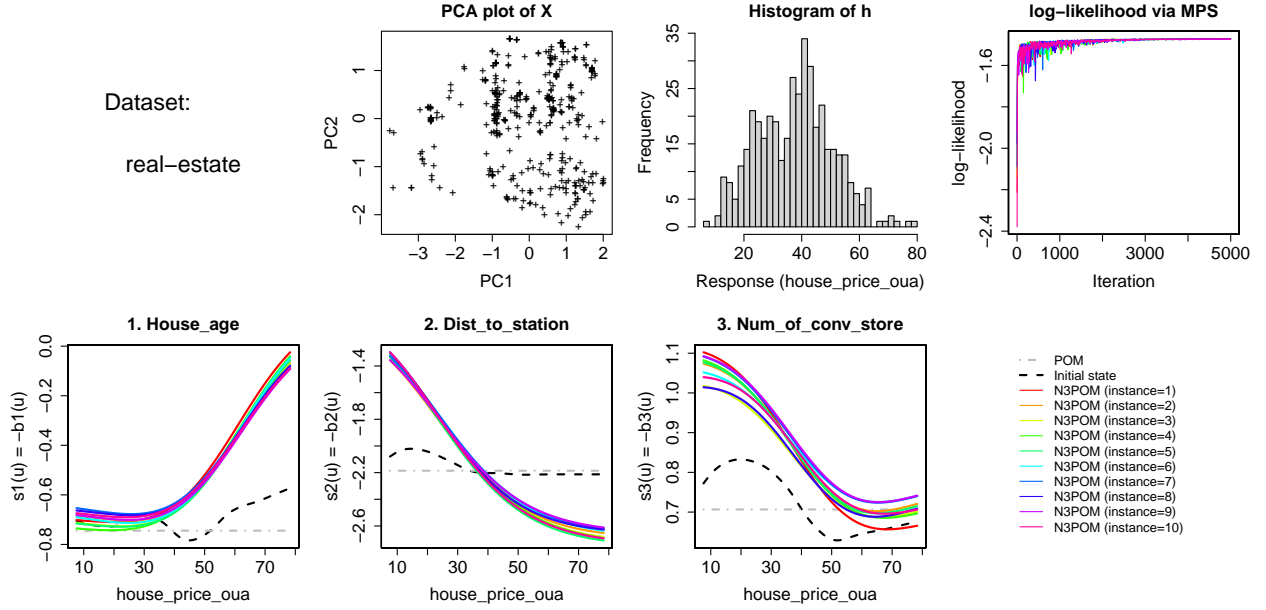
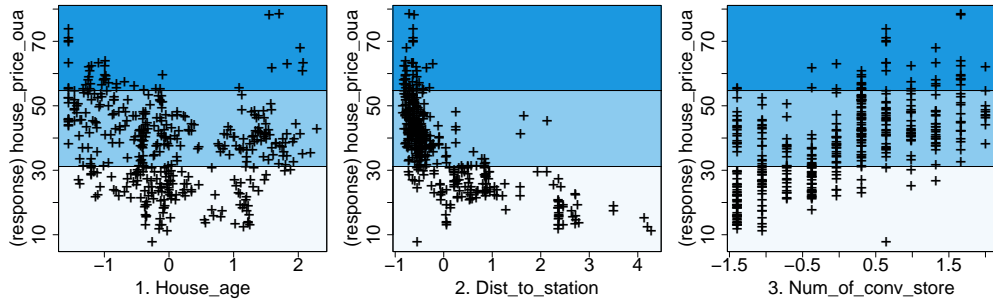


Figure 4: autoMPG8 dataset experiment.



(a) Experimental results.



(b) Scatter plots between covariates (house age, distance to station, and number of stores; x -axis) and response (house price of unit area; y -axis). Higher price, middle price, and lower price houses are separately colored.

Figure 5: real-estate dataset.

Acknowledgement

A. Okuno was supported by JST CREST (JPMJCR21N3) and JSPS KAKENHI (21K17718, 22H05106). K. Harada was supported by JSPS KAKENHI (21J10457). We would like to thank Keisuke Yano, Kohei Hattori, Shuichi Kawano, and Kei Hirose for their helpful discussions. We would like to also thank Lucas Kook for his positive comments and reference information.

A Gradient

With respect to the parameter θ , gradients $\nabla_{\theta} f_u, \nabla_{\theta} f_u^{[1]}$ of the prediction model f_u and its weak derivative $f_u^{[1]}$ are shown in Appendix A.1, A.2, respectively; together with these gradients, we show the gradient of the log-likelihood in Appendix A.3.

A.1 Gradient of the regression model

Let

$$\llbracket z \rrbracket = \begin{cases} 0 & (z < 0) \\ z & (z \in [0, 1]) \\ 1 & (z > 1) \end{cases}, \quad z \in \mathbb{R}.$$

Considering the identity

$$a(u) = \phi + \sum_{r=2}^R |\varphi_r| \left\llbracket \frac{u - j_{r-1}}{j_r - j_{r-1}} \right\rrbracket,$$

the gradient $\nabla_{\theta} f_u(\mathbf{x}_i)$ is obtained element-wise as: for $r^{\dagger} \in \{2, 3, \dots, R\}, k^{\dagger} \in [d], \ell^{\dagger} \in [L]$ and $u \in \mathcal{U}$,

$$\begin{aligned} \frac{\partial}{\partial \phi} f_u(\mathbf{x}_i) &= 1, \\ \frac{\partial}{\partial \varphi_{r^{\dagger}}} f_u(\mathbf{x}_i) &= \text{sign}(\varphi_{r^{\dagger}}) \left\llbracket \frac{u - j_{r^{\dagger}-1}}{j_{r^{\dagger}} - j_{r^{\dagger}-1}} \right\rrbracket, \\ \frac{\partial}{\partial v_{k^{\dagger}, \ell^{\dagger}}^{(1)}} f_u(\mathbf{x}_i) &= x_{ik^{\dagger}} \frac{\partial}{\partial v_{k^{\dagger}, \ell^{\dagger}}^{(1)}} b_{k^{\dagger}}(u) = x_{ik^{\dagger}} w_{k^{\dagger}, \ell^{\dagger}}^{(2)} \rho^{[1]}(w_{k^{\dagger}, \ell^{\dagger}}^{(1)} u + v_{k^{\dagger}, \ell^{\dagger}}^{(1)}), \\ \frac{\partial}{\partial v_{k^{\dagger}}^{(2)}} f_u(\mathbf{x}_i) &= x_{ik^{\dagger}} \frac{\partial}{\partial v_{k^{\dagger}}^{(2)}} b_{k^{\dagger}}(u) = x_{ik^{\dagger}}, \\ \frac{\partial}{\partial w_{k^{\dagger}, \ell^{\dagger}}^{(1)}} f_u(\mathbf{x}_i) &= x_{ik^{\dagger}} \frac{\partial}{\partial w_{k^{\dagger}, \ell^{\dagger}}^{(1)}} b_{k^{\dagger}}(u) = x_{ik^{\dagger}} w_{k^{\dagger}, \ell^{\dagger}}^{(2)} u \rho^{[1]}(w_{k^{\dagger}, \ell^{\dagger}}^{(1)} u + v_{k^{\dagger}, \ell^{\dagger}}^{(1)}), \\ \frac{\partial}{\partial w_{k^{\dagger}, \ell^{\dagger}}^{(2)}} f_u(\mathbf{x}_i) &= x_{ik^{\dagger}} \frac{\partial}{\partial w_{k^{\dagger}, \ell^{\dagger}}^{(2)}} b_{k^{\dagger}}(u) = x_{ik^{\dagger}} \rho(w_{k^{\dagger}, \ell^{\dagger}}^{(1)} u + v_{k^{\dagger}, \ell^{\dagger}}^{(1)}). \end{aligned}$$

A.2 Gradient of the weak derivative of the prediction model

Considering the identities

$$a^{[1]}(u) = \sum_{r=2}^R \mathbb{1}(u \in \mathcal{U}_{r-1}) \frac{|\varphi_r|}{j_r - j_{r-1}}, \quad b_k^{[1]}(u) = \sum_{\ell=1}^L w_{k, \ell}^{(2)} w_{k, \ell}^{(1)} \rho^{[1]}(w_{k, \ell}^{(1)} u + v_{k, \ell}^{(1)}),$$

the gradient $\nabla_{\theta} f_u^{[1]}(\mathbf{x})$ of the weak derivative $f_u^{[1]}(\mathbf{x})$ of the prediction model $f_u(\mathbf{x})$ is obtained element-wise as follows: for $r^{\dagger} \in \{2, 3, \dots, R\}, k^{\dagger} \in [d], \ell^{\dagger} \in [L]$ and $u \in \mathcal{U}$, we have

$$\frac{\partial}{\partial \phi} f_u^{[1]}(\mathbf{x}_i) = 0,$$

$$\begin{aligned}
\frac{\partial}{\partial \varphi_{r^\dagger}} f_u^{[1]}(\mathbf{x}_i) &= \mathbb{1}(u \in \mathcal{U}_{r^\dagger-1}) \frac{\text{sign}(\varphi_{r^\dagger})}{j_{r^\dagger} - j_{r^\dagger-1}}, \\
\frac{\partial}{\partial v_{k^\dagger, \ell^\dagger}^{(1)}} f_u^{[1]}(\mathbf{x}_i) &= x_{ik^\dagger} \frac{\partial}{\partial v_{k^\dagger, \ell^\dagger}^{(1)}} b_{k^\dagger}^{[1]}(u) = x_{ik^\dagger} w_{k^\dagger, \ell^\dagger}^{(2)} w_{k^\dagger, \ell^\dagger}^{(1)} \rho^{[2]}(w_{k^\dagger, \ell^\dagger}^{(1)} u + v_{k^\dagger, \ell^\dagger}^{(1)}), \\
\frac{\partial}{\partial v_{k^\dagger}^{(2)}} f_u^{[1]}(\mathbf{x}_i) &= x_{ik^\dagger} \frac{\partial}{\partial v_{k^\dagger}^{(2)}} b_{k^\dagger}^{[1]}(u) = 0, \\
\frac{\partial}{\partial w_{k^\dagger, \ell^\dagger}^{(1)}} f_u^{[1]}(\mathbf{x}_i) &= x_{ik^\dagger} \frac{\partial}{\partial w_{k^\dagger, \ell^\dagger}^{(1)}} b_{k^\dagger}^{[1]}(u) = x_{ik^\dagger} w_{k^\dagger, \ell^\dagger}^{(2)} w_{k^\dagger, \ell^\dagger}^{(1)} u \rho^{[2]}(w_{k^\dagger, \ell^\dagger}^{(1)} u + v_{k^\dagger, \ell^\dagger}^{(1)}) \\
&\quad + x_{ik^\dagger} w_{k^\dagger, \ell^\dagger}^{(2)} \rho^{[1]}(w_{k^\dagger, \ell^\dagger}^{(1)} u + v_{k^\dagger, \ell^\dagger}^{(1)}), \\
\frac{\partial}{\partial w_{k^\dagger, \ell^\dagger}^{(2)}} f_u^{[1]}(\mathbf{x}_i) &= x_{ik^\dagger} \frac{\partial}{\partial w_{k^\dagger, \ell^\dagger}^{(2)}} b_{k^\dagger}^{[1]}(u) = x_{ik^\dagger} w_{k^\dagger, \ell^\dagger}^{(1)} \rho^{[1]}(w_{k^\dagger, \ell^\dagger}^{(1)} u + v_{k^\dagger, \ell^\dagger}^{(1)}).
\end{aligned}$$

A.3 Gradient of the log-likelihood

Using the conditional probability density function (8), we get

$$\begin{aligned}
\nabla_{\boldsymbol{\theta}} \ell_{\boldsymbol{\zeta}}(\boldsymbol{\theta}) &= \sum_{i=1}^n \zeta_i \nabla_{\boldsymbol{\theta}} \log q(h_i | \mathbf{x}_i) \\
&= \sum_{i=1}^n \zeta_i \nabla_{\boldsymbol{\theta}} \{\log \sigma^{[1]}(f_{h_i}(\mathbf{x}_i)) + \log f_{h_i}^{[1]}(\mathbf{x}_i)\} \\
&= \sum_{i=1}^n \zeta_i \left\{ \frac{\sigma^{[2]}(f_{h_i}(\mathbf{x}_i))}{\sigma^{[1]}(f_{h_i}(\mathbf{x}_i))} \nabla_{\boldsymbol{\theta}} f_{h_i}(\mathbf{x}_i) + \frac{1}{f_{h_i}^{[1]}(\mathbf{x}_i)} \nabla_{\boldsymbol{\theta}} f_{h_i}^{[1]}(\mathbf{x}_i) \right\}.
\end{aligned}$$

Together with the gradient of f_u and $f_u^{[1]}$, the gradient of the log-likelihood is obtained element-wise as follows: For $r^\dagger \in \{2, 3, \dots, R\}$, $k^\dagger \in [d]$, $\ell^\dagger \in [L]$, we have

$$\begin{aligned}
\frac{\partial}{\partial \phi} \ell_{\boldsymbol{\zeta}}(\boldsymbol{\theta}) &= \sum_{i=1}^n \zeta_i \frac{\sigma^{[2]}(f_{h_i}(\mathbf{x}_i))}{\sigma^{[1]}(f_{h_i}(\mathbf{x}_i))}, \\
\frac{\partial}{\partial \varphi_{r^\dagger}} \ell_{\boldsymbol{\zeta}}(\boldsymbol{\theta}) &= \text{sign}(\varphi_{r^\dagger}) \sum_{i=1}^n \zeta_i \frac{\sigma^{[2]}(f_{h_i}(\mathbf{x}_i))}{\sigma^{[1]}(f_{h_i}(\mathbf{x}_i))} \left\| \frac{h_i - j_{r^\dagger-1}}{j_{r^\dagger} - j_{r^\dagger-1}} \right\| \\
&\quad + \frac{\text{sign}(\varphi_{r^\dagger})}{j_{r^\dagger} - j_{r^\dagger-1}} \sum_{i=1}^n \zeta_i \mathbb{1}(h_i \in \mathcal{U}_{r^\dagger-1}) \frac{1}{f_{h_i}^{[1]}(\mathbf{x}_i)}, \\
\frac{\partial}{\partial v_{k^\dagger, \ell^\dagger}^{(1)}} \ell_{\boldsymbol{\zeta}}(\boldsymbol{\theta}) &= \sum_{i=1}^n \zeta_i \frac{\sigma^{[2]}(f_{h_i}(\mathbf{x}_i))}{\sigma^{[1]}(f_{h_i}(\mathbf{x}_i))} x_{ik^\dagger} w_{k^\dagger, \ell^\dagger}^{(2)} w_{k^\dagger, \ell^\dagger}^{(1)} \rho^{[1]}(w_{k^\dagger, \ell^\dagger}^{(1)} h_i + v_{k^\dagger, \ell^\dagger}^{(1)}) \\
&\quad + \sum_{i=1}^n \zeta_i \frac{1}{f_{h_i}^{[1]}(\mathbf{x}_i)} x_{ik^\dagger} w_{k^\dagger, \ell^\dagger}^{(2)} w_{k^\dagger, \ell^\dagger}^{(1)} \rho^{[2]}(w_{k^\dagger, \ell^\dagger}^{(1)} h_i + v_{k^\dagger, \ell^\dagger}^{(1)}), \\
\frac{\partial}{\partial v_{k^\dagger}^{(2)}} \ell_{\boldsymbol{\zeta}}(\boldsymbol{\theta}) &= \sum_{i=1}^n \zeta_i \frac{\sigma^{[2]}(f_{h_i}(\mathbf{x}_i))}{\sigma^{[1]}(f_{h_i}(\mathbf{x}_i))} x_{ik^\dagger}, \\
\frac{\partial}{\partial w_{k^\dagger, \ell^\dagger}^{(1)}} \ell_{\boldsymbol{\zeta}}(\boldsymbol{\theta}) &= \sum_{i=1}^n \zeta_i \frac{\sigma^{[2]}(f_{h_i}(\mathbf{x}_i))}{\sigma^{[1]}(f_{h_i}(\mathbf{x}_i))} x_{ik^\dagger} w_{k^\dagger, \ell^\dagger}^{(2)} h_i \rho^{[1]}(w_{k^\dagger, \ell^\dagger}^{(1)} h_i + v_{k^\dagger, \ell^\dagger}^{(1)}) \\
&\quad + \sum_{i=1}^n \zeta_i \frac{1}{f_{h_i}^{[1]}(\mathbf{x}_i)} \left\{ x_{ik^\dagger} w_{k^\dagger, \ell^\dagger}^{(2)} w_{k^\dagger, \ell^\dagger}^{(1)} h_i \rho^{[2]}(w_{k^\dagger, \ell^\dagger}^{(1)} h_i + v_{k^\dagger, \ell^\dagger}^{(1)}) \right.
\end{aligned}$$

$$\begin{aligned}
& + x_{ik^\dagger} w_{k^\dagger, \ell^\dagger}^{(2)} \rho^{[1]}(w_{k^\dagger, \ell^\dagger}^{(1)} h_i + v_{k^\dagger, \ell^\dagger}^{(1)}) \}, \\
\frac{\partial}{\partial w_{k^\dagger, \ell^\dagger}^{(2)}} \ell \zeta(\boldsymbol{\theta}) &= \sum_{i=1}^n \zeta_i \frac{\sigma^{[2]}(f_{h_i}(\mathbf{x}_i))}{\sigma^{[1]}(f_{h_i}(\mathbf{x}_i))} x_{ik^\dagger} \rho(w_{k^\dagger, \ell^\dagger}^{(1)} h_i + v_{k^\dagger, \ell^\dagger}^{(1)}) \\
& + \sum_{i=1}^n \zeta_i \frac{1}{f_{h_i}^{[1]}(\mathbf{x}_i)} x_{ik^\dagger} w_{k^\dagger, \ell^\dagger}^{(1)} \rho^{[1]}(w_{k^\dagger, \ell^\dagger}^{(1)} h_i + v_{k^\dagger, \ell^\dagger}^{(1)}).
\end{aligned}$$

B Initialization

With given parameter vectors $\hat{\boldsymbol{\beta}}_j = (\hat{\beta}_{j1}, \hat{\beta}_{j2}, \dots, \hat{\beta}_{jd})^\top$ ($j = 1, 2, \dots, J$), which are preliminarily computed using the existing algorithm for (discrete) NPOM, we initialize the neural network parameters to satisfy

$$b_k(j) \approx \hat{\beta}_{jk}, \quad (j = 1, 2, \dots, J; k = 1, 2, \dots, d). \quad (19)$$

In our implementation, we employ the vectors $\hat{\boldsymbol{\beta}}_1, \hat{\boldsymbol{\beta}}_2, \dots, \hat{\boldsymbol{\beta}}_{J-1}$ computed by `serp` package in R language and specify $\hat{\boldsymbol{\beta}}_J = \hat{\boldsymbol{\beta}}_{J-1} + (\hat{\boldsymbol{\beta}}_{J-1} - \hat{\boldsymbol{\beta}}_{J-2}) = 2\hat{\boldsymbol{\beta}}_{J-1} - \hat{\boldsymbol{\beta}}_{J-2}$ formally.

To satisfy the equality (19), we employ an NN using sigmoid activation function $\rho(z) = 1/(1 + \exp(-z))$ and $L > d$; with a sufficiently large constant T (e.g., $T = 10$, satisfying $\rho(-T) \approx 0, \rho(+T) \approx 1$), we define

$$\begin{aligned}
v_k^{(2)} &= \frac{1}{J} \sum_{j=1}^J \hat{\beta}_{jk}, \\
v_{k, \ell}^{(1)} &= \begin{cases} -T\ell & (\ell \in \{1, 2, \dots, J\}) \\ 0 & (\text{Otherwise}) \end{cases}, \\
w_{k, \ell}^{(1)} &= \begin{cases} T & (\ell \in \{1, 2, \dots, J\}) \\ 0 & (\text{Otherwise}) \end{cases}, \\
w_{k, \ell}^{(2)} &= \begin{cases} \frac{\hat{\beta}_{\ell k} - v_k^{(2)} - \sum_{\ell_1=1}^{\ell-1} w_{k, \ell_1}^{(2)}}{\rho(0)} & (\ell \in \{1, 2, \dots, J\}) \\ 0 & (\text{Otherwise}) \end{cases},
\end{aligned}$$

for all $k \in \{1, 2, \dots, d\}$. Next, we have

$$\begin{aligned}
b_k(j) &= \sum_{\ell=1}^L w_{k, \ell}^{(2)} \rho(w_{k, \ell}^{(1)} j + v_{k, \ell}^{(1)}) + v_k^{(2)} \\
&= \sum_{\ell=1}^J w_{k, \ell}^{(2)} \rho(T(j - \ell)) + v_k^{(2)} \\
&\approx \sum_{\ell=1}^J w_{k, \ell}^{(2)} \{\rho(-\infty) \mathbb{1}(j < \ell) + \rho(0) \mathbb{1}(\ell = j) + \rho(\infty) \mathbb{1}(\ell < j)\} + v_k^{(2)} \\
&= w_{k, j}^{(2)} \rho(0) + \sum_{\ell=1}^{j-1} w_{k, \ell}^{(2)} + v_k^{(2)} \\
&= \frac{\hat{\beta}_{jk} - v_k^{(2)} - \sum_{\ell=1}^{j-1} w_{k, \ell}^{(2)}}{\rho(0)} \rho(0) + \sum_{\ell=1}^{j-1} w_{k, \ell}^{(2)} + v_k^{(2)} \\
&= \hat{\beta}_{jk}.
\end{aligned}$$

For more stability in the NN training in our implementation, the non-zero weights in $\{w_{k, \ell}^{(2)}\}$ divided by $T = \max_{t \in \mathbb{N}} \{L/J \geq t\}$ are duplicated T times. Furthermore, the non-zero weights in $\{w_{k, \ell}^{(1)}\}, \{v_{k, \ell}^{(1)}\}$ are also duplicated T times. I.i.d. standard normal random numbers are added to the remaining zero-weights.

Following this duplication, the weights are more uniformly distributed compared to the setting in which only a few non-zero weights exist. Accordingly, the subsequent neural network training is expected to be more stable.

C Proofs

Proof of Proposition 1. We employ a proof by contradiction. Given that \mathcal{U} is a compact set, $s := \text{esssup}_{u \in [1, J]} a^{[1]}(u) > 0$ holds. Suppose there exists $(u', \mathbf{x}') \in \mathcal{U} \times \mathbb{R}^d$ such that $|\nabla_u \langle \mathbf{b}(u'), \mathbf{x}' \rangle| > 0$. Thus, we may assume $t_{u', \mathbf{x}'} := \nabla_u \langle \mathbf{b}(u'), \mathbf{x}' \rangle > 0$ without loss of generality (consider $-\mathbf{x}'$ instead of $\nabla_u \langle \mathbf{b}(u'), \mathbf{x}' \rangle < 0$). Next, by taking $L := (s/t_{u', \mathbf{x}'} + 1)$, we get

$$\nabla_u f_{u'}(-L\mathbf{x}') < s - L \nabla_u \langle \mathbf{b}(u'), \mathbf{x}' \rangle < s - (\{s/t_{u', \mathbf{x}'}\} + 1) t_{u', \mathbf{x}'} = -t_{u', \mathbf{x}'} < 0$$

almost surely. At point $-L\mathbf{x}'$, $f_u(-L\mathbf{x})$ is decreasing with respect to u , over a sufficiently small open ball around u' . Thus, a contradiction is derived. Accordingly, $|\nabla_u \langle \mathbf{b}(u), \mathbf{x} \rangle| = 0$ holds for all $(u, \mathbf{x}) \in \mathcal{U} \times \mathbb{R}^d$. Together with the continuity of the function \mathbf{b} , $\mathbf{b}(u)$ is a constant function. \square

Proof of Proposition 2. Given that the weak derivative is obtained as

$$\langle \mathbf{b}^{[1]}(u), \mathbf{x} \rangle = \sum_{k=1}^d x_k b_k^{[1]}(u) = \sum_{k=1}^d x_k \sum_{\ell=1}^L w_{k,\ell}^{(2)} w_{k,\ell}^{(1)} \rho^{[1]}(w_{k,\ell}^{(1)} u + v_{k,\ell}^{(1)}),$$

The Cauchy-Schwarz inequality proves an inequality

$$\begin{aligned} |\langle \mathbf{b}^{[1]}(u), \mathbf{x} \rangle| &\leq \sqrt{\sum_{k=1}^d x_k^2} \sqrt{\sum_{k=1}^d \left\{ \sum_{\ell=1}^L w_{k,\ell}^{(2)} w_{k,\ell}^{(1)} \rho^{[1]}(w_{k,\ell}^{(1)} u + v_{k,\ell}^{(1)}) \right\}^2} \\ &< \eta \cdot \rho_\infty^{[1]} \cdot \sqrt{\sum_{k=1}^d \left\{ \sum_{\ell=1}^L |w_{k,\ell}^{(2)} w_{k,\ell}^{(1)}| \right\}^2} \end{aligned} \quad (20)$$

for $\mathbf{x} = (x_1, x_2, \dots, x_d) \in \mathcal{X}_2(\eta)$. This inequality indicates that

$$f_u^{[1]}(\mathbf{x}) = a^{[1]}(u) + \langle \mathbf{b}^{[1]}(u), \mathbf{x} \rangle \stackrel{(20)}{\geq} \min_{r=2,3,\dots,R-1} s_{r-1} - \eta \cdot \rho_\infty^{[1]} \cdot \sqrt{\sum_{k=1}^d \left\{ \sum_{\ell=1}^L |w_{k,\ell}^{(2)} w_{k,\ell}^{(1)}| \right\}^2} \stackrel{(15)}{\geq} 0,$$

where the non-negativity of the right-most side is obtained based on the inequality (15). Given that $f_u^{[1]}$ is a weak derivative of the function f_u , f_u is non-decreasing. Given that the above calculation holds for all \mathbf{x} , the continuity of f_u proves the assertion. \square

References

- Agarwal, R., Melnick, L., Frosst, N., Zhang, X., Lengerich, B., Caruana, R., and Hinton, G. (2021). Neural additive models: Interpretable machine learning with neural nets. In *Advances in Neural Information Processing Systems*, pages 4699–4711.
- Agresti, A. (2010). *Analysis of Ordinal Categorical Data*. John Wiley & Sons.
- Agresti, A. and Tarantola, C. (2018). Simple ways to interpret effects in modeling ordinal categorical data. *Statistica Neerlandica*, 72(3):210–223.

- Baumann, P. F. M., Hothorn, T., and Rügamer, D. (2021). Deep conditional transformation models. In *Machine Learning and Knowledge Discovery in Databases. Research Track*, pages 3–18. Springer International Publishing.
- Bennett, S. (1983). Log-logistic regression models for survival data. *Journal of the Royal Statistical Society. Series C (Applied Statistics)*, 32(2):165–171.
- Cardoso, J. S. and da Costa, J. F. P. (2007). Learning to classify ordinal data: The data replication method. *Journal of Machine Learning Research*, 8:1393–1429.
- Chu, W. and Ghahramani, Z. (2005). Gaussian processes for ordinal regression. *Journal of Machine Learning Research*, 6(35):1019–1041.
- Cybenko, G. (1989). Approximation by superpositions of a sigmoidal function. *Mathematics of Control, Signals and Systems*, 2(4):303–314.
- Daniels, H. and Velikova, M. (2010). Monotone and partially monotone neural networks. *IEEE Transactions on Neural Networks*, 21(6):906–917.
- Dua, D. and Graff, C. (2017). UCI machine learning repository.
- Farouki, R. T. (2012). The bernstein polynomial basis: A centennial retrospective. *Computer Aided Geometric Design*, 29(6):379–419.
- Goodfellow, I., Bengio, Y., and Courville, A. (2016). *Deep Learning*. MIT Press. <http://www.deeplearningbook.org>.
- Hastie, T. and Tibshirani, R. (1993). Varying-coefficient models. *Journal of the Royal Statistical Society. Series B (Methodological)*, 55(4):757–796.
- Herzog, L., Kook, L., Gotschi, A., Petermann, K., Hansel, M., Hamann, J., Durr, O., Wegener, S., and Sick, B. (2022). Deep transformation models for functional outcome prediction after acute ischemic stroke. *Biometrical Journal*.
- Kalbfleisch, J. D. and Prentice, R. L. (2002). *The Statistical Analysis of Failure Time Data*. John Wiley & Sons, Inc., 2nd edition.
- Kook, L., Baumann, P. F., Dürr, O., Sick, B., and Rügamer, D. (2022a). Estimating conditional distributions with neural networks using r package deeptrafo. *arXiv preprint [arXiv:2211.13665](https://arxiv.org/abs/2211.13665)*.
- Kook, L., Herzog, L., Hothorn, T., Durr, O., and Sick, B. (2022b). Deep and interpretable regression models for ordinal outcomes. *Pattern Recognition*, 122:108263.
- Liu, Q., Shepherd, B. E., Li, C., and Harrell, Jr, F. E. (2017). Modeling continuous response variables using ordinal regression. *Statistics in Medicine*, 36(27):4316–4335.
- Liu, X., Han, X., Zhang, N., and Liu, Q. (2020). Certified monotonic neural networks. In *Advances in Neural Information Processing Systems*, volume 33, pages 15427–15438.
- Long, J. S. and Freese, J. (2006). *Regression models for categorical dependent variables using Stata*, volume 7. Stata press.
- Lu, F., Ferraro, F., and Raff, E. (2022). Continuously generalized ordinal regression for linear and deep models. In *Proceedings of the 2022 SIAM International Conference on Data Mining (SDM)*, pages 28–36.
- McCullagh, P. (1980). Regression models for ordinal data. *Journal of Royal Statistical Society. Series B (Methodological)*, 42(2):109–127.

- McCullagh, P. and Nelder, J. A. (1989). *Generalized Linear Models*. Chapman & Hall CRC, London.
- Peterson, B. and Harrell, F. E. (1990). Partial proportional odds models for ordinal response variables. *Journal of Royal Statistical Society. Series C (Applied Statistics)*, 39(2):205–217.
- Satoh, K., Tonda, T., and Izumi, S. (2016). Logistic regression model for survival time analysis using time-varying coefficients. *American Journal of Mathematical and Management Sciences*, 35(4):353–360.
- Sick, B., Hathorn, T., and Durr, O. (2021). Deep transformation models: Tackling complex regression problems with neural network based transformation models. In *Proceedings of the 25th International Conference on Pattern Recognition*, pages 2476–2481.
- Sill, J. (1997). Monotonic networks. In *Advances in Neural Information Processing Systems*, volume 10.
- Thas, O., Neve, J. D., Clement, L., and Ottoy, J.-P. (2012). Probabilistic index models. *Journal of Royal Statistical Society. Series B (Methodological)*, 74(4):623–671.
- Tutz, G. and Berger, M. (2022). Sparser ordinal regression models based on parametric and additive location-shift approaches. *International Statistical Review*, 90(2):306–327.
- Tutz, G. and Gertheiss, J. (2016). Regularized regression for categorical data. *Statistical Modelling*, 16(3):161–200.
- Ugba, E. R., Mörlin, D., and Gertheiss, J. (2021). Smoothing in ordinal regression: An application to sensory data. *Stats*, 4(3):616–633.
- Vargas, V. M., Gutiérrez, P. A., and Hervás, C. (2019). Deep ordinal classification based on the proportional odds model. In *From Bioinspired Systems and Biomedical Applications to Machine Learning*, pages 441–451.
- Vargas, V. M., Gutierrez, P. A., and Hervas-Martinez, C. (2020). Cumulative link models for deep ordinal classification. *Neurocomputing*, 401:48–58.
- Williams, R. (2006). Generalized ordered logit/partial proportional odds models for ordinal dependent variables. *Stata Journal*, 6(1):58–82.
- Williams, R. (2016). Understanding and interpreting generalized ordered logit models. *The Journal of Mathematical Sociology*, 40(1):7–20.
- Wurm, M. J., Rathouz, P. J., and Hanlon, B. M. (2021). Regularized ordinal regression and the ordinalNet R package. *Journal of Statistical Software*, 99(6):1–42.
- You, S., Ding, D., Canini, K., Pfeifer, J., and Gupta, M. (2017). Deep lattice networks and partial monotonic functions. In *Advances in Neural Information Processing Systems*, volume 30.

Supplementary material:

“An interpretable neural network-based non-proportional odds model for ordinal regression”.

A. Okuno (*okuno@ism.ac.jp*) and K. Harada (*haradak@tokyo-med.ac.jp*).

D Additional experiments.

In addition to the autoMPG6, autoMPG8, and real-estate datasets used in the main body of the study, we collected boston-housing, concrete, and airfoil datasets from the UCI machine learning repository (Dua and Graff, 2017). We train the N^3 POM by leveraging these datasets described in the following section and their results are shown in Figures 6–8.

The existing `serp` function used for initializing the N^3 POM is time-consuming for larger datasets. Therefore, for datasets with $n > 2000$, we first choose 2000 samples uniformly and randomly. Next, we apply the `serp` function to the selected samples for initialization. Subsequently, we apply the MPS algorithm to train the N^3 POM using the entire dataset.

boston-housing ($n = 506, d = 12$). The boston-housing dataset consists of 12 covariates (“`crim`” (continuous), “`zn`” (continuous), “`indus`” (continuous), “`chas`” (binary), “`nox`” (continuous), “`rm`” (continuous), “`age`” (continuous), “`dis`” (continuous), “`rad`” (discrete), “`tax`” (continuous), “`ptratio`” (continuous), “`lstat`” (continuous)) and a continuous response (“`medv`”) representing the housing price in boston. We preliminarily removed the “black” row for fairness. Descriptions of the covariates are provided in the caption of Figure 6.

concrete ($n = 1030, d = 8$). The concrete dataset consists of eight covariates (“`Cement`” (continuous), “`BlastFurnaceSlag`” (continuous), “`FlyAsh`” (continuous), “`Water`” (continuous), “`Superplasticizer`” (continuous), “`CoarseAggregate`” (continuous), “`FineAggregate`” (continuous), “`Age`” (continuous)) and a continuous response (“`ConcreteCompressiveStrength`”).

airfoil ($n = 1503, d = 5$). The airfoil dataset consists of 5 covariates (frequency in hertz “`freq`” (continuous), angle of attack in degrees “`angle`” (continuous), chord length in meters “`chord`” (continuous), free-stream velocity in meters “`velocity`” (continuous), suction side displacement thickness in meters “`disp. thickness`” (continuous) and a continuous response, “sound pressure” representing the scaled sound pressure level in decibels.

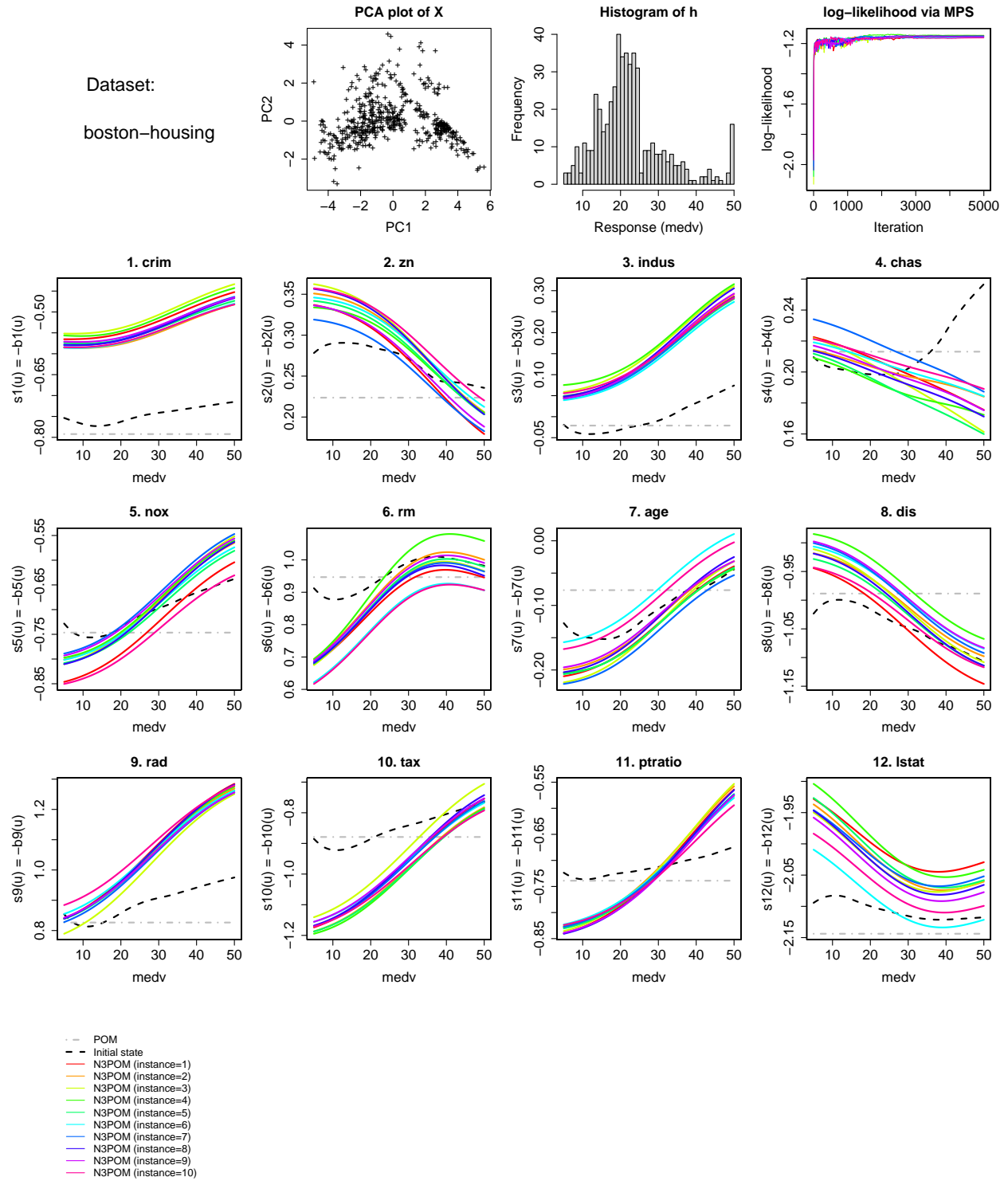


Figure 6: Boston-housing dataset experiment.

(**Covariates**) **crim**: per capita crime rate by town, **zn**: proportion of residential land zoned for lots over 25,000 sq.ft, **indus**: proportion of non-retail business acres per town, **chas**: Charles River dummy variable (=1 the house is located next to the river; 0 otherwise), **nox**: nitric oxides concentration (parts per 10 million), **rm**: average number of rooms per dwelling, **age**: proportion of owner-occupied units built prior to 1940, **dis**: weighted distances to five Boston employment centers, **rad**: index of accessibility to radial highways, **tax**: full-value property-tax rate per \$10,000, **ptratio**: pupil-teacher ratio by town, **lstat**: lower status of the population.

(**Response**) **medv**: Median value of owner-occupied homes in \$1000's.

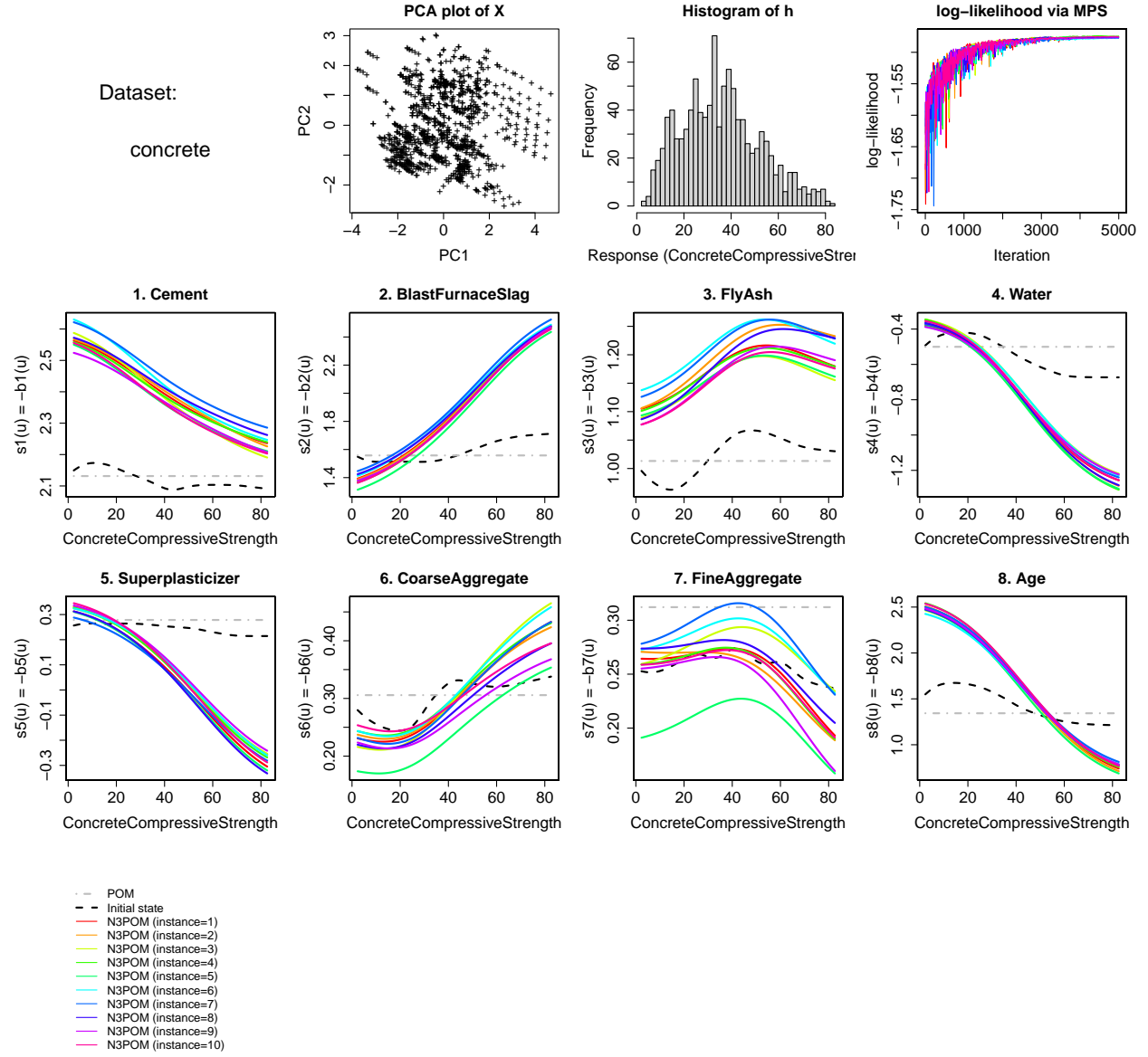


Figure 7: concrete dataset experiment.

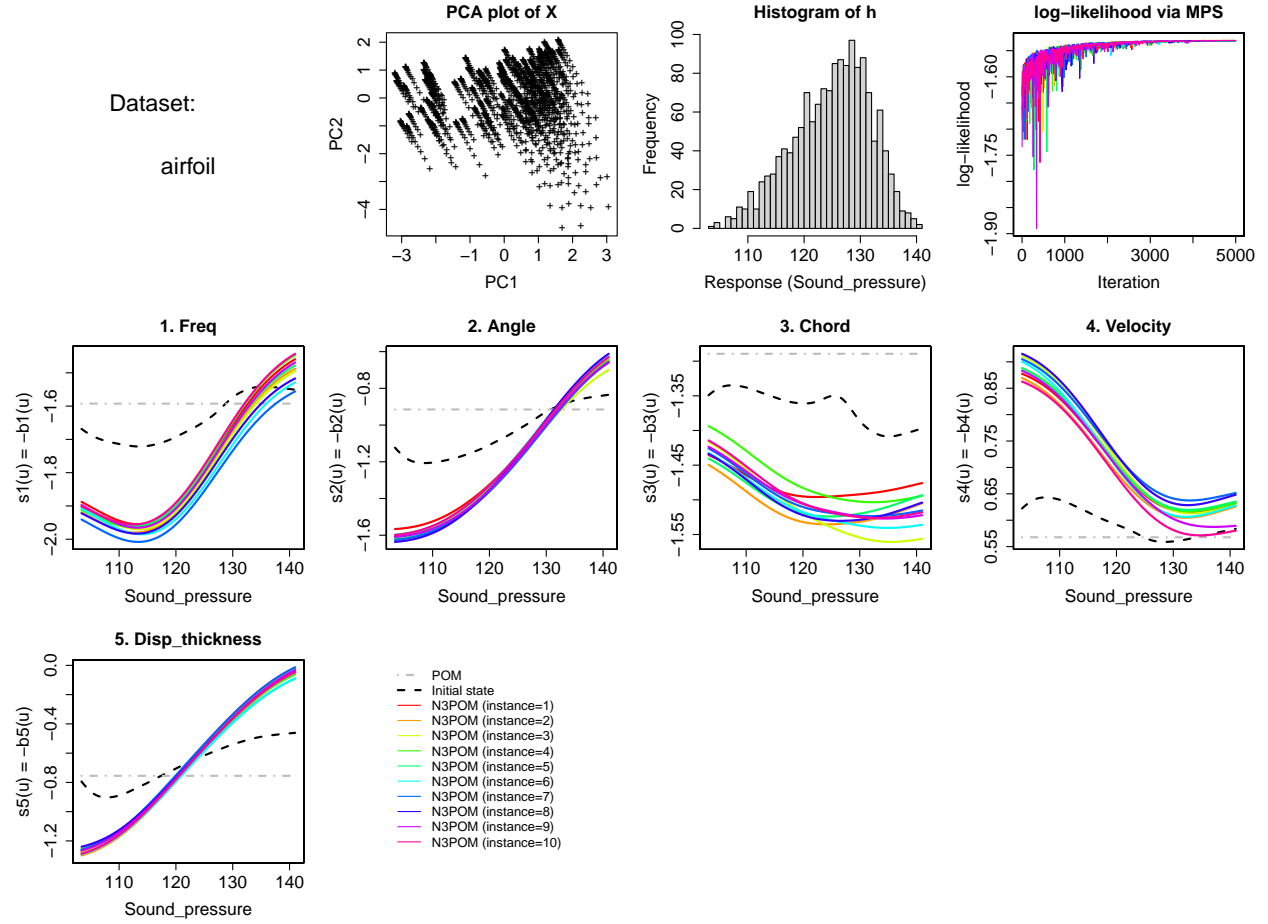


Figure 8: airfoil dataset experiment.

E Summary of datasets.

The covariates and response in autoMPG8, real-estate, boston-housing, concrete, airfoil, and cycle powerplant datasets are summarized in Figures 9–13. These plots are generated by `pairs.panels` function in `psych` package¹. Therein, the scatter plots for each pair of covariates and their correlation coefficients are provided. We omit the plot for autoMPG6 because it is completely subsumed in autoMPG8. Note that the covariates and responses are preliminarily standardized by following the procedure described in Section 5.1.

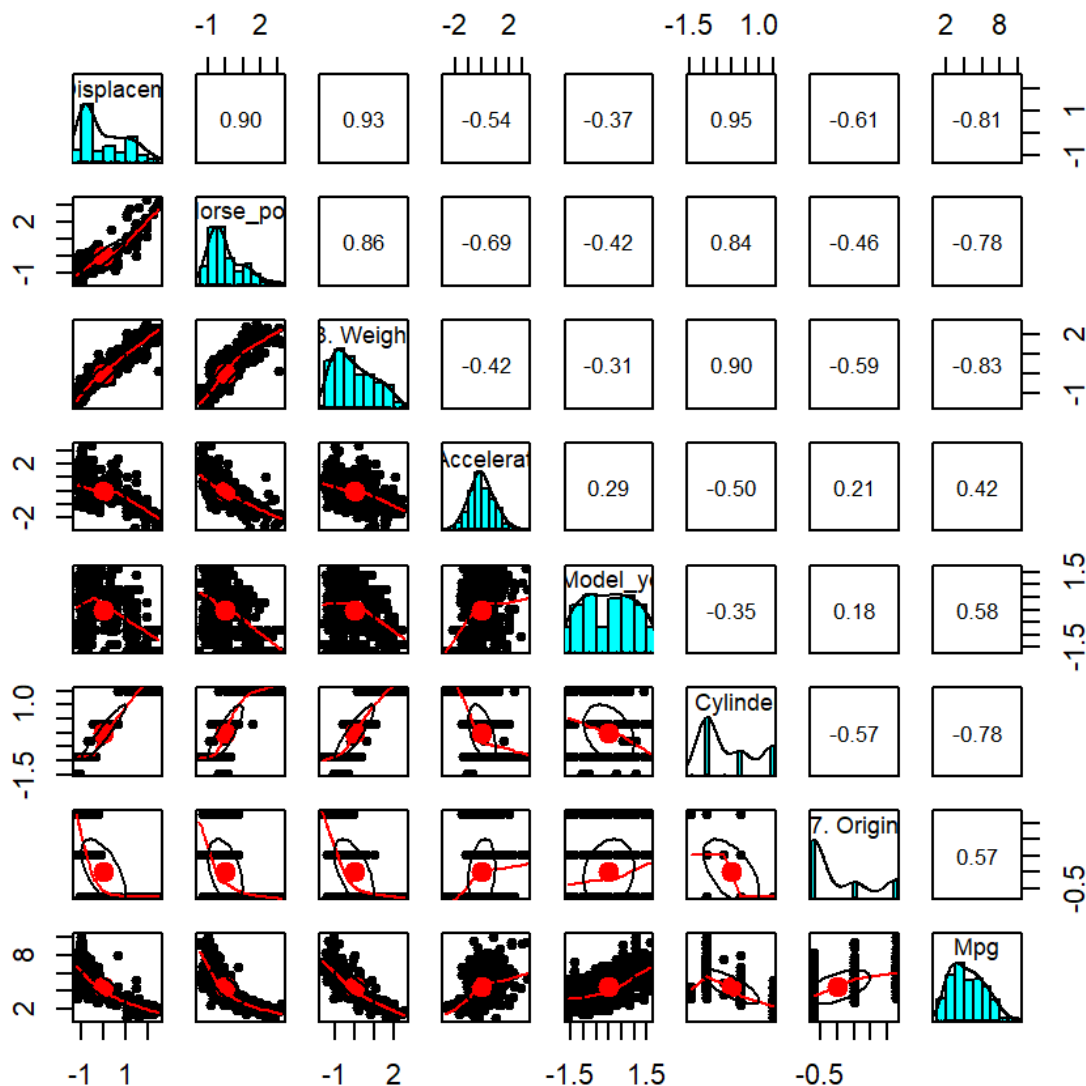


Figure 9: Summary of autoMPG8 dataset (subsuming autoMPG6 dataset).

¹<https://cran.r-project.org/package=psych>

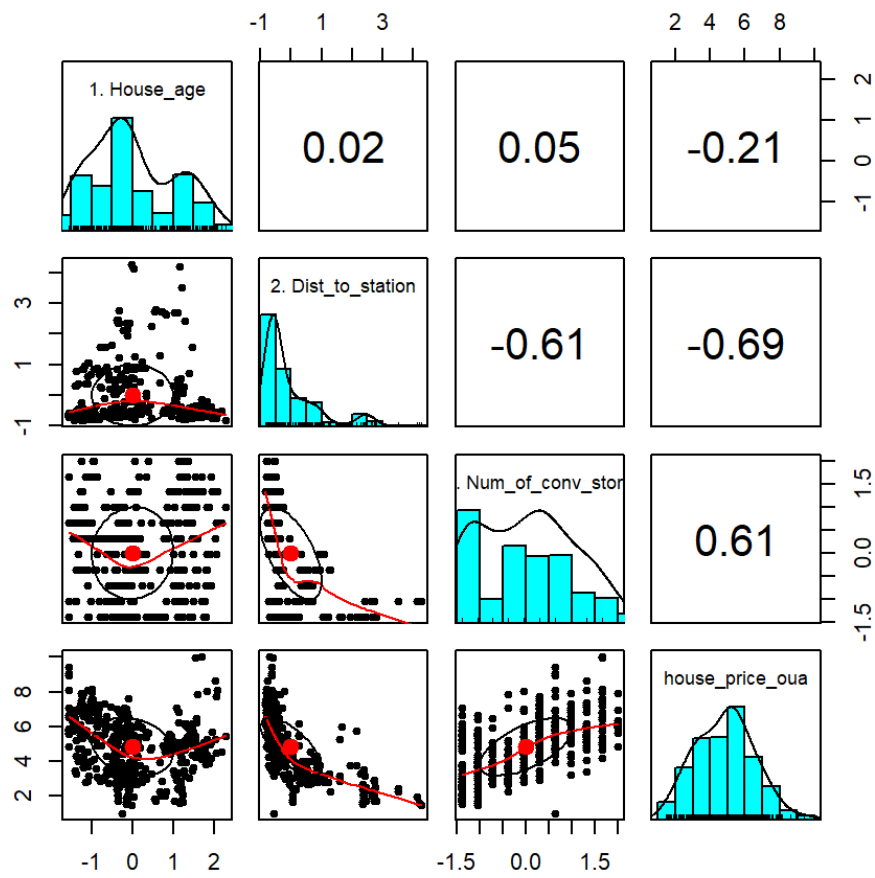


Figure 10: Summary of the real-estate dataset.

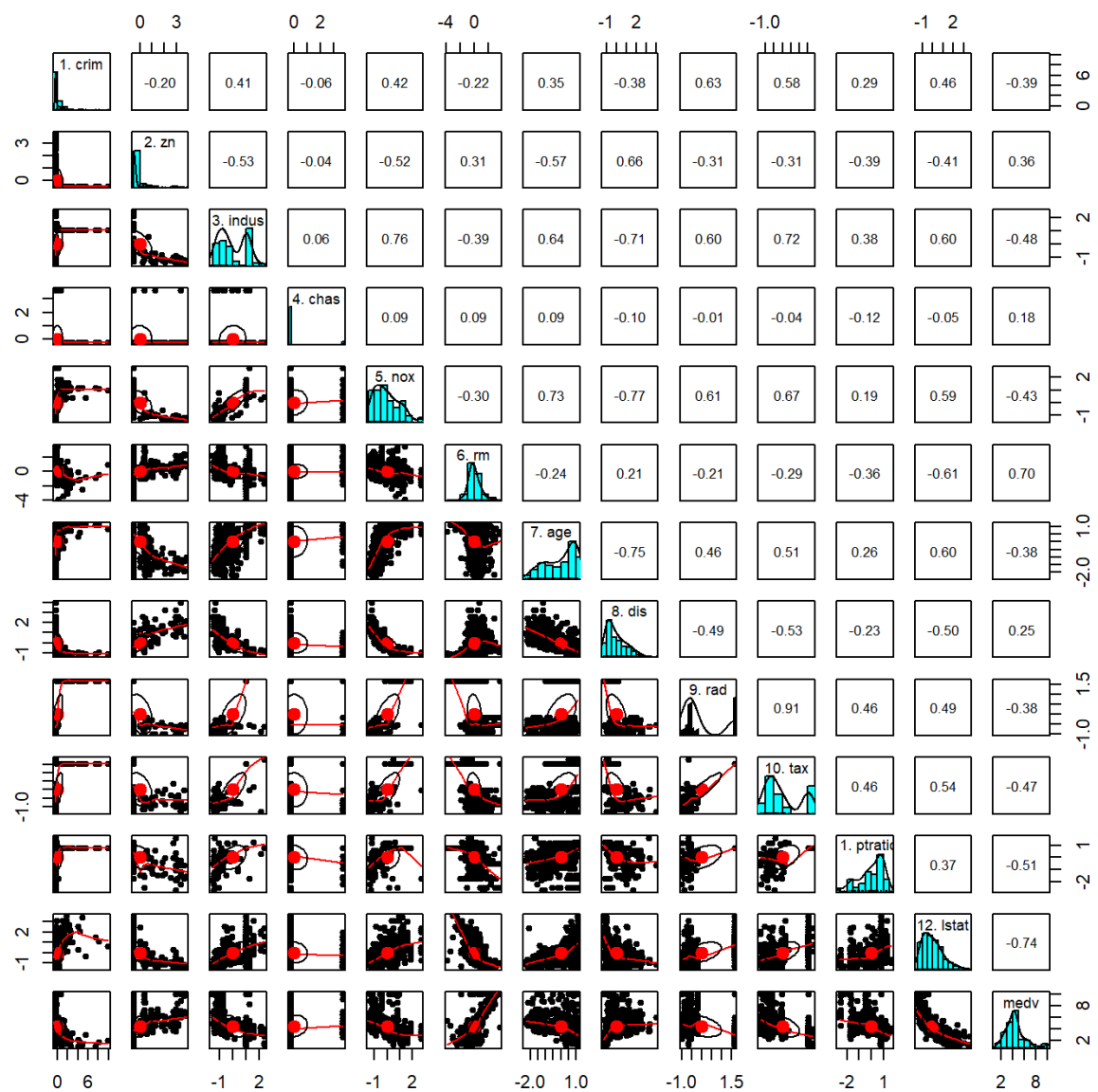


Figure 11: Summary of the boston-housing dataset.

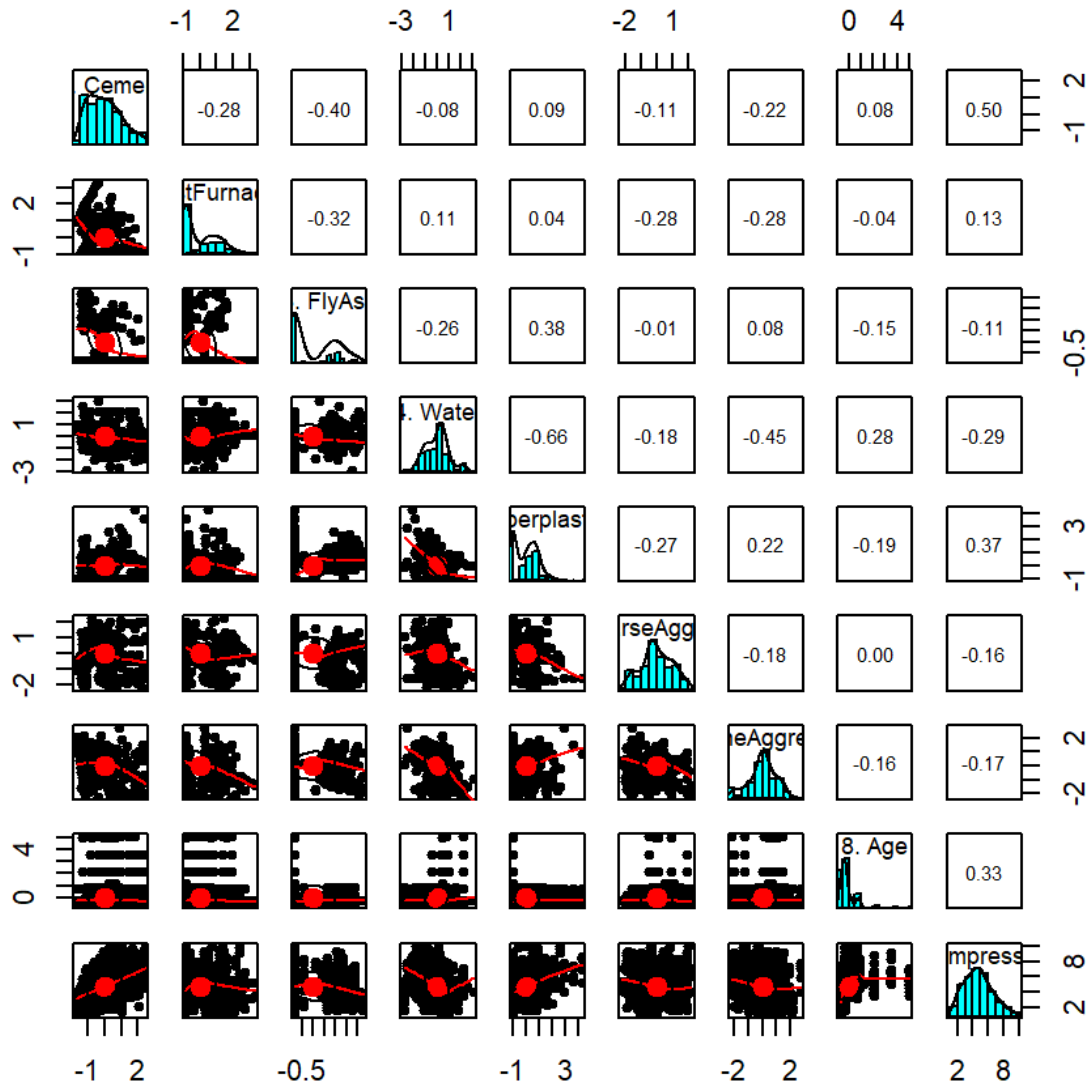


Figure 12: Summary of the concrete dataset.

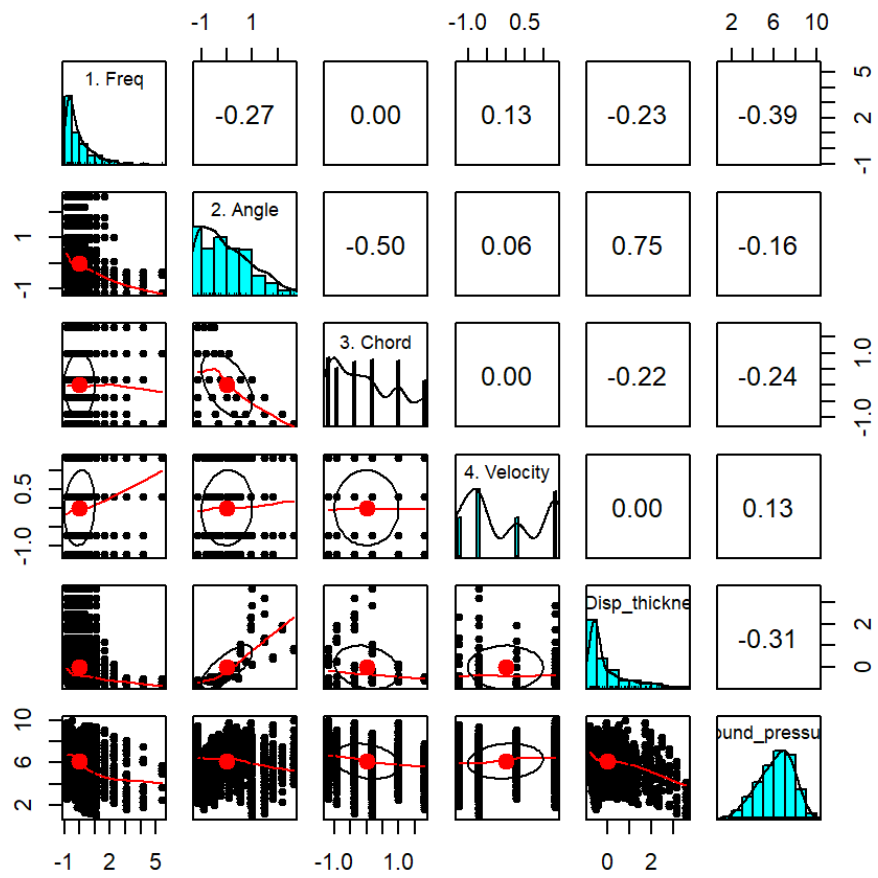


Figure 13: Summary of the airfoil dataset.